Geochemistry, Sr-Nd isotopes and zircon U-Pb geochronology of intrusive rocks: Constraint on the genesis of the Cheshmeh Khuri Cu mineralization and its link with granitoids in the Lut Block, Eastern Iran

Maryam Javidi Moghaddam, Mohammad Hassan Karimpour, Azadeh Malekzadeh Shafaroudi, José Francisco Santos, Maria Helena Mendes

PII: S0375-6742(18)30435-7
DOI: https://doi.org/10.1016/j.gexplo.2019.04.001
Reference: GEXPLO 6299

To appear in: *Journal of Geochemical Exploration*

Received date: 3 August 2018
Revised date: 24 January 2019
Accepted date: 2 April 2019

Please cite this article as: M.J. Moghaddam, M.H. Karimpour, A.M. Shafaroudi, et al., Geochemistry, Sr-Nd isotopes and zircon U-Pb geochronology of intrusive rocks: Constraint on the genesis of the Cheshmeh Khuri Cu mineralization and its link with granitoids in the Lut Block, Eastern Iran, Journal of Geochemical Exploration, https://doi.org/10.1016/j.gexplo.2019.04.001

Geochemistry, Sr-Nd Isotopes and Zircon U–Pb Geochronology of Intrusive Rocks: Constraint on the Genesis of the Cheshmeh Khuri Cu Mineralization and its Link with Granitoids in the Lut Block, Eastern Iran

Maryam Javidi Moghaddam: Department of Geology, Faculty of Science, Ferdowsi University of Mashhad, P.O. Box No. 91775-1436, Mashhad, Iran.

Email: Javidi.maryam@mail.um.ac.ir

* Mohammad Hassan Karimpour: Department of Geology and Research Center for Ore Deposit of Eastern Iran, Faculty of Science, Ferdowsi University of Mashhad, P.O. Box No. 91775-1436, Mashhad, Iran.

Email: karimpur@um.ac.ir

Azadeh Malekzadeh Shafaroudi: Department of Geology and Research Center for Ore Deposit of Eastern Iran, Faculty of Science, Ferdowsi University of Mashhad, P.O. Box No. 91775-1436, Mashhad, Iran.

Email: Shafaroudi@um.ac.ir

José Francisco Santos: Department of Geosciences, Geobiotec Research unit, University of Aveiro, 3810-193 Aveiro, Portugal.

Email: jfsantos@ua.pt

Maria Helena Mendes: Department of Geosciences, Geobiotec Research unit, University of Aveiro, 3810-193 Aveiro, Portugal.

mmendes@ua.pt

Abstract

The Cheshmeh Khuri prospecting area, part of the Tertiary volcanic-plutonic rocks in the Lut Block (central eastern Iran), comprises Middle Eocene granitoid and volcanic (with basaltic andesite to rhyolite composition) sequences that intruded pyroclastic rocks. Copper mineralization is related to the granitoid rocks. The mafic rocks occur mainly as dykes and are related to a younger magmatic activity (post-mineralization) in the area. The main hydrothermal alteration zones include quartz-sericite-pyrite±carbonate (QSP±C), argillic, and propylitic. Mineralization (pyrite, chalcocite, chalcopyrite, sphalerite, galena and magnetite) occurs as disseminated, stockwork and vein-type. The granitoids have features typical of high-K calk-alkaline, metaluminous, and belong to magnetite granitoid series. Primitive mantle normalized trace element spider diagrams display enrichment in LILE, such as Rb, Ba, and Cs, compared to those of HFSE. Chondrite-normalized REE plots show moderately to slightly strong LREE enriched patterns, and a negligible negative Eu anomaly. Rb–Sr whole rock–feldspar–biotite-hornblende and zircon U–Pb ages between ~44.6 and ~43.4 Ma (Middle Eocene) were obtained in granitoid samples. Initial $^{87}Sr/^{86}Sr$ ratios of granitoids range from 0.7047 to 0.7054, and their εNd_i values vary from -1.1 to +0.8. Initial $^{87}Sr/^{86}Sr$ ratios of mafic rocks range from 0.7043 to 0.7047, and the εNd_i values vary from +0.7 to +3.5. The whole set of geochemical data of rocks in the study area indicate an origin of the parental melts in a subduction-modified upper mantle in post-collisional extension-related zone. The primitive magmas of granitoids underwent

contamination and assimilation through being exposed to the continental crust, while primitive magmas of the mafic rocks do not have relevant crustal contribution. The geochemical and radiogenic isotope data for the granitoids associated with mineralization in the Cheshmeh Khuri area in comparison with those of other prospects in the Lut Block indicate that mantle has played a crucial role in their petrogeneses and metallogeneses. Due to the crustal contamination and assimilation, the proportion of mantle component that was involved in the granitic magma shows a decrease in the Cheshmeh Khuri area. It seems that the Cheshmeh Khuri area has the lowest potential for a significant amount of Cu–Au agglomeration.

Keywords: Geochemistry; Sr-Nd isotopes; Rb-Sr and U-Pb geochronology; Copper mineralization; Cheshmeh Khuri; Lut Block.

1. Introduction

The Lut Block, in eastern Central Iranian Microcontinent, extends over 900Km in a N-S direction from the Doruneh Fault in the north to the Jaz-Mourian basin in the south and is about 200Km wide in the E-W direction from the Nehbandan Fault in the east to the Naybandan Fault in the west (Berberian and King, 1981; Karimpour and Stern, 2009) (Fig. 1). Extensive magmatic activity in the Lut Block, is spatially and temporally associated with several types of mineralization events and the episode of Middle Eocene to lower Oligocene (43.3–33.3 Ma) is very important in terms of magmatism and mineralization (Karimpour et al., 2012).

Three main zones of porphyry copper deposits in Iran consist of Kerman (central SE Iran), Azerbaijan (NW Iran) and the Lut Block (E Iran). Studies of exploration, fluid evolution, magma source and the genetic type in porphyry copper deposits have mainly focused on Kerman (e.g., Hezarkhani et al., 1999; McInnes et al., 2005; Mirnejad et al., 2013; Mohajjel et al., 2003; Shafiei et al., 2008; Shahabpour, 2007) and Azerbaijan (e.g., Aghazadeh et al., 2015; Jamali et al., 2010;

Maghsoudi et al., 2014) deposits. In comparison, less attention has been paid to copper deposits in the Lut Block which have mainly occurred during Late Eocene to Early Oligocene (Arjmandzadeh and Santos, 2014; Malekzadeh Shafaroudi, 2009; Richards et al., 2012).

The prospecting area is located in a significant part of the Lut Block that includes many cases of Cu-Ag±Pb±Zn vein- type mineralization, such as Shikasteh Sabz, Mire-e-Khash, Rashidi, Shurk, Ghar-e-Kaftar and Howz-e-Dagh (Javidi Moghaddam et al., 2018; Lotfi, 1982; Rowshanravan, 2006) in the neighboring areas, as well as in the kaolin deposit (the Cheshmeh Khuri area). The Geochemistry of volcanic rocks in the Cheshmeh Khuri district was generally described by Lotfi (1982). Tarkian et al. (1983) have implemented Rb-Sr dating in the Cheshmeh Khuri district on the andesite unit. Recently, Salim (2012) has studied petrography and geochemistry of volcanic rocks in the central part of the Cheshmeh Khuri district.

Until now, no detailed studies of the Cheshmeh-Khuri copper mineralization and associated granitoid rocks have been conducted. In this paper, we present and discuss geochemical (both elemental and isotopic) and geochronological (Rb–Sr and U-Pb) data in order to provide a comprehensive understanding of age, origin and petrogenesis of granitoid rocks, and to determine their relationship with Cu mineralization in the study area. Moreover, geochemical and Sr–Nd isotopic analyses of mafic were performed to assist in the discussion of the petrogenesis of the igneous rocks in the Cheshmeh Khuri area.

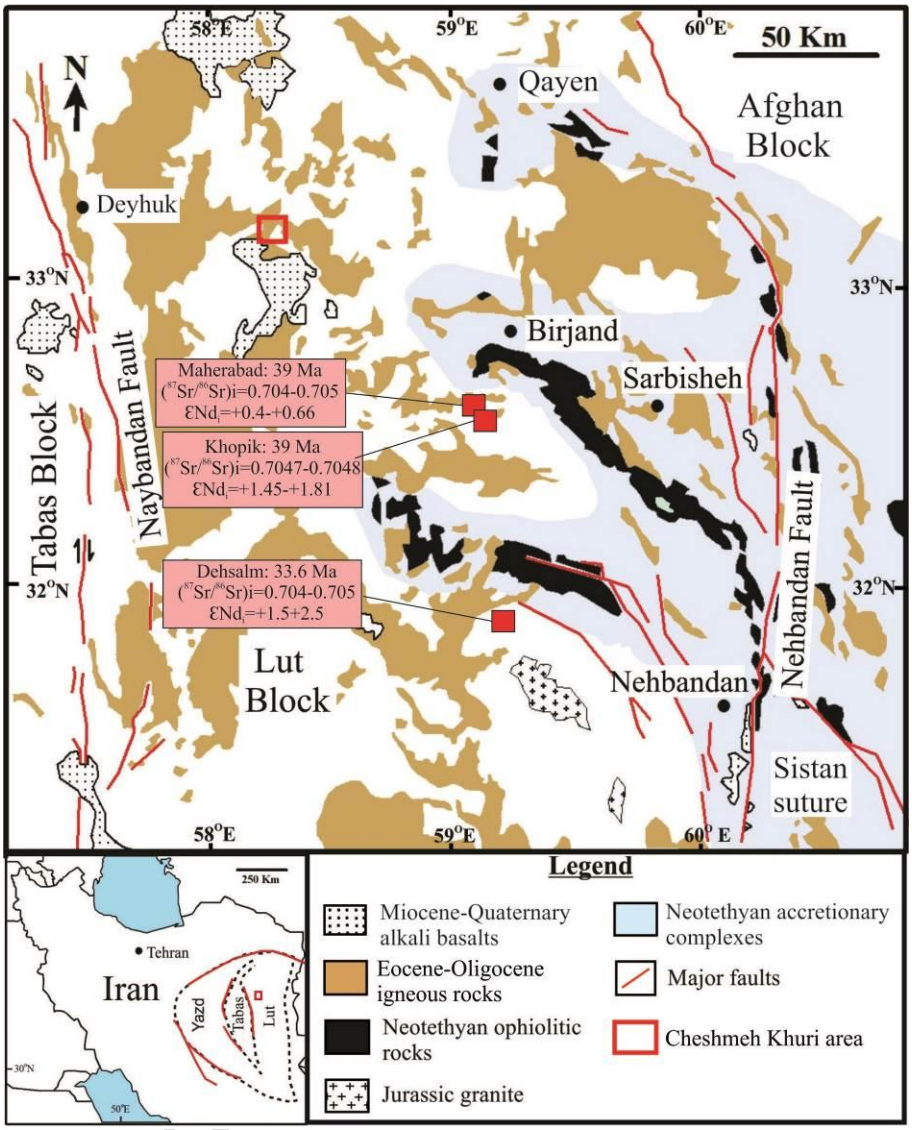

Fig. 1 Geological sketch map of the Lut–Sistan region, eastern Iran and the location of the study area (bounded by red frame) (modified from Pang et al., 2012). Location and the results of the dating and Sr-Nd isotopes on different porphyry copper prospects (Arjmandzadeh and Santos, 2014; Malekzadeh Shafaroudi, 2009; Malekzadeh Shafaroudi et al., 2015) are shown .Inset shows location of the Lut Block in map of Iran.

2. Geological setting

The Cheshmeh Khuri prospecting area belongs to the Tertiary metallogenic volcano–plutonic rocks of the Lut Block, between 33°08′ and 33°15′ north latitude and 58°20′ and 58°27′ east longitude and is located at 111 km NW of Birjand city, Khorasan Jonoubi Province, Eastern Iran (Fig. 1). The oldest unit in the Cheshmeh Khuri area includes Upper Jurassic conglomerate which crops out in the southwest of the study area (Fig. 2).

Most of the Cheshmeh Khuri area is occupied by Middle Eocene volcanic rocks (Lotfi, 1995). These rocks can be divided into the following two groups: 1- pyroclastic rocks (rhyolitic tuff breccia and andesitic tuff breccia), which are intruded by granitoid rocks in some places, and 2- basaltic andesite to dacite rocks (Fig. 2). Rhyolitic tuff breccia has been exposed in the southern and eastern parts of the Cheshmeh Khuri area. These units contain 25 to 75% lithic fragments of 64 to 120 mm in diameter with rhyolitic composition. Andesitic tuff breccia crops out in the southern and eastern parts of the Cheshmeh Khuri deposit. These units consist of lithic fragments (25 to 75%) of 64 to 85 mm in diameter and mainly have andesitic composition. Sequence of intermediate to felsic volcanic rocks includes basaltic andesite, trachyandesite, andesite and dacite. Dacite has small outcrops in the northern and southern parts of the area with massive and flow structures. Andesite unit has the most expansion than that of other volcanic units and crops out in the west and southwest of the area (Fig. 2). In the Cheshmeh Kuri area, Rb–Sr age of 39.3 Ma (Tarkian et al., 1983) was obtained for the andesite unit.

Intrusive rocks are emplaced into the pyroclastic units as stocks and dykes. Based on the relationship with mineralization, they can be divided into two groups: granitoid (diorite porphyry and granodiorite porphyry) and mafic rocks (gabbro, gabbrodiorite porphyry and monzodiorite porphyry) rocks. Granitoid rocks that are related to the mineralization, mainly occur as stocks and crop out at the central and southeast of the study area. Diorite porphyry stocks are the largest

granitoid rocks that outcrop in the central part of the area. Mafic rocks crop out mostly at the eastern part of the study area. These rocks are younger than mineralization, and show less alteration than the previous group (Fig. 2).

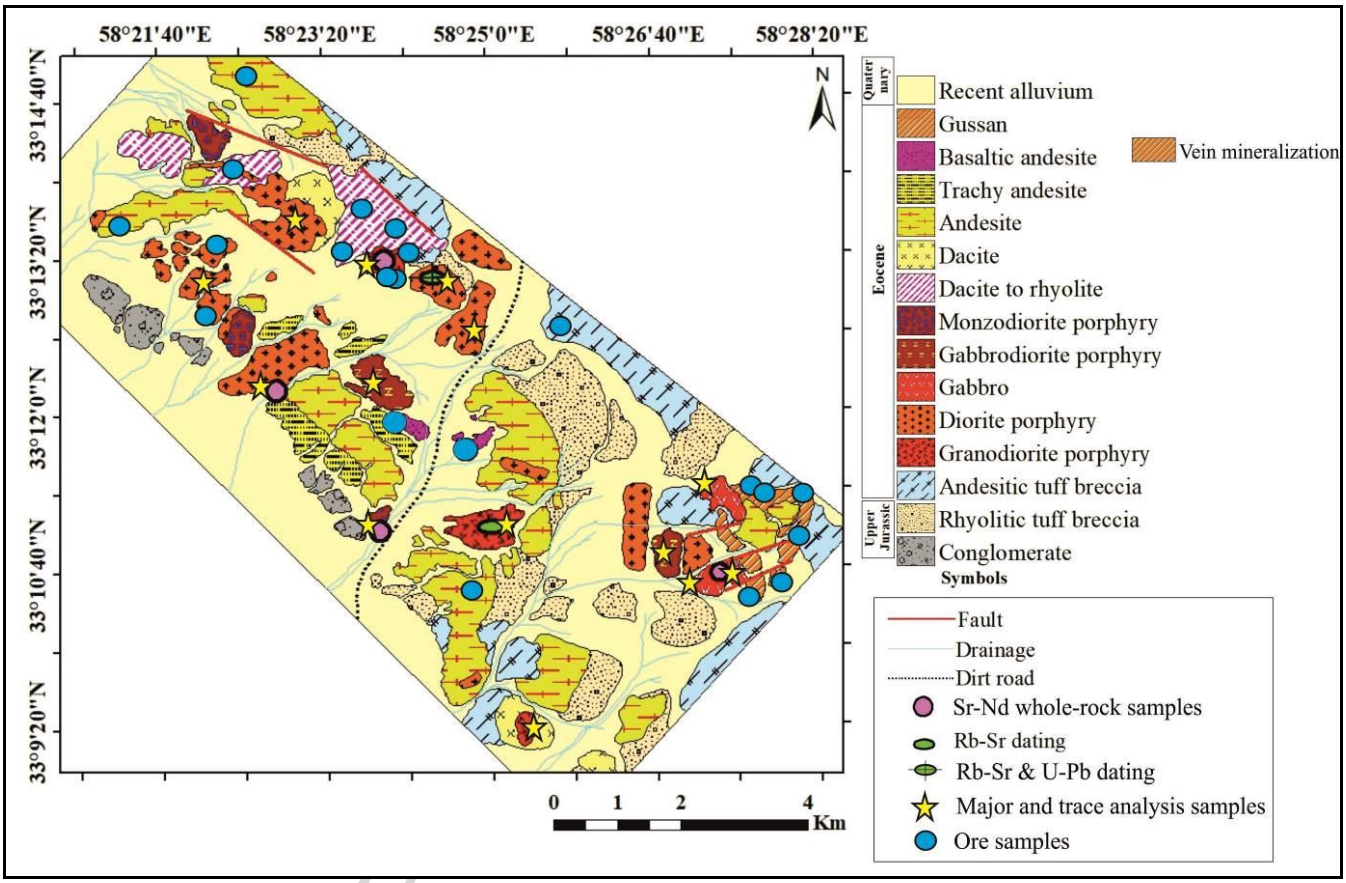

Fig. 2 Geological map of Cheshmeh Khuri area, showing locations of Sr–Nd whole-rock, Rb-Sr dating, U-Pb dating and ore samples.

3. Sampling and analytical methods

After field work, a total of 270 thin sections and polished slabs from volcanic and intrusive rocks and ore samples were studied by an optical microscope. After their petrographic study, samples were selected for further XRD, geochemical and isotopic studies. In addition, the magnetic susceptibility of intrusive rocks was measured.

3.1. XRD analysis

The X-ray diffraction technique is one of the most essential identification tools for identification of clay minerals. For this purpose, eight samples taken from the argillic alteration zone and the kaolin deposit were analyzed using the X-Ray Diffractometry (XRD) techniques at the Analytical Geology Lab. of the Spectrum Kansaran Binaloud in Iran. A sufficient amount of sample should be utilized to yield approximately 5 to 10 g of clay (<2μm fraction).

3.2. Geochemical analysis

Metal concentrations of 21 samples selected from the vein and disseminated mineralization were analyzed at the IMPRC laboratory of Iran using Inductively Coupled plasma-Mass/Optical Emission Spectroscopy (ICP-OES) techniques. The Au content of the samples was analyzed by fire assay (Table 1).

3.3. Major and trace element analysis

Fourteen samples (14 intrusive rocks) were collected from representative, least-altered or fresh rocks for major and trace element analyses. The samples were analyzed for major elements by wavelength-dispersive X-Ray Fluorescence (XRF) spectrometry using fused disks and the Philips PW 1410 XRF spectrometer at the Analytical Geology Lab. of Spectrum Kansaran Binaloud in Iran. Trace elements and REE analyses were determined by Inductively Coupled Plasma Mass Spectrometry (ICP-MS) at the ACME Analytical Laboratories (Vancouver) Ltd., Canada. Powdered samples (0.2 g) were fused by lithium metaborate/tetraborate flux and digested by nitric acid before determination by ICP-MS. Whole rock analytical results for major element oxides and trace elements are listed in Table 2.

3.4. Rb–Sr and Sm–Nd isotopic analysis

Sr and Nd isotopic compositions were determined for six whole-rock samples and five separate minerals (two of plagioclase, two of hornblende and one of biotite) of the Cheshmeh Khuri intrusive and volcanic rocks at the Laboratório de Geologia Isotópica da Universidade de Aveiro, Portugal. Plagioclase, hornblende and biotite from sample CH20 and plagioclase and hornblende from sample CH14 were separated using magnetic separation procedures and purified by handpicking under a binocular microscope. They were rinsed using pure water and crushed several times to remove mineral inclusions and then powdered in agate mortar.

The selected powdered samples were dissolved by HF/HNO_3 solution in Teflon Parr acid digestion bombs at 200º C temperatures for 3 days. After evaporation of the final solution, the samples were dissolved by HCl (6N) and dried again. The elements to analyze were purified using the conventional ion chromatography technique in two stages: 1) separation of Sr from REE elements in ion exchange column by means of AG8 50W Bio-Rad cation exchange resin; 2) purification of Nd from other lanthanides elements in columns by means of Ln Resin (ElChrom Technologies) cation exchange resin. All reagents used in the preparation of the samples were sub-boiling distilled, and the water was produced by a Milli-Q Element (Millipore) apparatus. Sr was loaded on a single Ta filament by H_3PO_4, whereas Nd was loaded on a Ta outer side filament with HCl in a triple filament arrangement. $^{87}Sr/^{86}Sr$ and $^{143}Nd/^{144}Nd$ isotopic ratios were determined using a Multi-Collector Thermal Ionization Mass Spectrometer (TIMS) VG Sector 54. The data were acquired in dynamic mode with peak measurements at 1–2 V for ^{88}Sr and 0.5–1.0 V for ^{144}Nd. Sr and Nd isotopic ratios were corrected for mass fractionation relative to $^{88}Sr/^{86}Sr = 0.1194$ and $^{146}Nd/^{144}Nd = 0.7219$. During this study, the SRM-987 standard gave an average value of $^{87}Sr/^{86}Sr = 0.710261$ (±17) (N = 13; conf. lim = 95%) and JNdi-1 standard gave an average value of $^{143}Nd/^{144}Nd = 0.5120970$ (±76) (N = 13; conf. lim = 95%). The element

concentrations (Rb and Sr) of separate minerals were determined by the Isotope Dilution Mass Spectrometry method (IDMS), using an $^{87}Rb/^{84}Sr$ and $^{150}Nd/^{149}Sm$ double spike. Rb-Sr isochrones were calculated using Isoplot 4 (Ludwig, 2012), with the value for ^{87}Rb decay constant recently recommended by IUPAC-IUGS (Villa et al., 2015). The Rb–Sr and Sm–Nd isotope compositions are listed in Table 3.

3.5. U–Pb zircon geochronology

One sample of diorite porphyry unit (CH20) was selected for U–Pb dating of zircon. Zircon crystals were isolated from the rock sample by using standard techniques involving crashing, washing, heavy liquid and handpicking using the binocular microscope techniques at the Ferdowsi University of Mashhad. The analyses were performed using a New Wave 193 nmArF laser ablation systemcoupled to a Nu PlasmaHR inductively coupled plasma-mass spectrometer (ICP-MS) at the Arizona Laserchron Center using the methods described by Gehrels et al. (2008).

3.6. Magnetic susceptibility measurements

Magnetic susceptibility of the intrusive rocks (150 in total) from the study area was measured by a GMS2 Sintrex device at the Ferdowsi University of Mashhad, Iran. The accuracy of this device is 1×10^{-7} SI.

4. Petrographical characteristics of intrusive rocks

According to cross-cutting relationships observed in the field and U-Pb and Rb-Sr dating, the lithology of the Cheshmeh Khuri area can be divided into the following five groups: 1- Upper Jurassic conglomerate, 2- Middle Eocene pyroclastic rocks, which are intruded by granitoid rocks, 3- Middle Eocene basaltic andesite to dacite rocks, 4- granitoid (diorite porphyry and granodiorite porphyry) rocks that are related to the mineralization and 5- mafic rocks (gabbro, gabbrodiorite porphyry and monzodiorite porphyry).

The intrusive rocks of the Cheshmeh Khuri area generally have porphyritic to granular textures with a range of fine to medium-grained groundmass. Five intrusive units based on the type and abundance of phenocrysts, groundmass and mafic minerals were identified in the Cheshmeh Khuri area. The volcanic and granitoid rocks have been mostly altered (quartz-sericite-pyrite±carbonate, argillic and propylitic), and contain different amounts of mineralization as disseminate and stockwork. Mafic rocks are younger than mineralization, and have no mineralization and less alteration.

4.1. Gabbro

This rock has a coarse grained granular texture with a grain size of 0.8–4 mm. The main minerals are 35–40 vol. % of plagioclase (labradorite: An59-An64), 25–30 vol. % of pyroxene (augite), 20-25 vol. % of olivine and nearly 3-5 vol. % of hornblende. Apatite is the most common accessory mineral, occurring in various forms from hexagonal to needle crystals as inclusions in plagioclase.

4.2. Gabbrodiorite porphyry

The gabbrodiorite porphyry displays porphyritic texture with coarse-grained groundmass and 40 vol. % of phenocrysts (0.4–2 mm in dimeter). The phenocrysts are mainly 20–25 vol. % of plagioclase, 7-10 vol. % of pyroxene (augite) and 3–5 vol. % of olivine. In this unit, plagioclase crystals change in composition from andesine (An45-An50) to labradorite (An50-An57). The matrix comprises plagioclase and pyroxene. The matrix is microcrystalline, which mostly comprises plagioclase and pyroxene and accessory minerals of magnetite, apatite and pyrite.

4.3. Monzodiorite porphyry

The monzodiorite porphyry has porphyritic texture with medium-grained groundmass and normally contains up to 38 vol.% of phenocrysts (0.2–1.2 mm in diameter), including 14–18

vol.% of plagioclase (andesine: (An38-An42)), 5– 7 vol.% of K-feldspar, 4–5 vol.% of hornblende, 2-4 vol.% of pyroxene and 2–4 vol.% of quartz. Clinopyroxene forms mostly as subhedral to euhedral grains that have a composition of augite. The same minerals, especially plagioclase and hornblende are also present in the groundmass. Accessory minerals include magnetite and apatite.

4.4. Diorie porphyry

These rocks display porphyritic texture with 30-37% of phenocrysts (0.4–1.2 mm in diameter) with medium-grained groundmass. Phenocrysts mainly consist of plagioclase (18–20 vol.%), K-feldspar (2– 4 vol.%), hornblende (2–4 vol.%), pyroxene (3-5 vol.%), biotite (2-4 vol.%) and quartz (2–3 vol.%). Composition of plagioclase is mainly of andesine (An35-An41). The matrix is cryptocrystalline and has the same mineral content as phenocrysts.

4.5. Granodiorite porphyry

The granodiorite porphyry has porphyritic texture with medium-grained groundmass and normally contains up to 50 vol.% of phenocrysts (0.3-1 mm in diameter). The phenocrysts are plagioclase (15-20 vol.%), which generally appears as zoned crystals, quartz (5-7 vol.%), K-feldspar (5-10 vol.%), biotite (5-7 vol.%) and hornblende (3-5 vol.%). The plagioclase in the granodiorite porphyry occurs oligoclase (An18-An23). The matrix is mostly quartz, plagioclase and K-feldspar. Biotite minerals generally show kinking and breaking as a result of tectonic deformation and stress. A few traces of magnetite and apatite are also present.

5. Alteration

Hydrothermal alteration is well-developed in the prospect area. Based on the field and petrography results, the alteration intensity of the host rocks (all exposed volcanic and intrusive rocks) may be represented by three groups of strongly (>60%), moderately (~10–60%), and

weakly (<10%) altered rocks. The main alteration types are quartz-sericite-pyrite±carbonate, argillic and propylitic. However, they are divided into sub-types based on their intensity as shown in the alteration map (Fig. 3).

Quartz-sericite-pyrite±carbonate (QSP±C) alteration is only exposed in the north part of the prospect area (trench) and affects granodiorite porphyry. The QSP±C alteration mainly consists of quartz, sericite, pyrite, and calcite as veinlets and replacement zones (Fig. 4a), sericite replacement of K-feldspar (55–60%) as veinlets (1-3%). In the surface rocks, the QSP±C alteration minerals are extensively replaced by supergene argillic alteration minerals, i.e. kaolinite, illite (X-ray powder diffraction (XRD) was used to identify the minerals), quartz, and Fe-oxyhydroxides.

Argillic alteration is widespread in the central section of the prospect area and affects the volcanic rocks (andesite and rhyolite) and parts of the diorite porphyry rocks (Fig. 3). The argillic alteration (Fig. 4b) consists of kaolinite, sericite, pyrite, minor quartz, chlorite, and epidote. The alteration intensity is very variable (<10% to 70-80%), reaching to the highest intensity in the southern part of the prospect area and forms the kaolin deposit (Fig. 4c). In the most intensely-altered rocks, the primary textures of the host rock have been destroyed and mostly replaced by clay minerals. Kaolinite and illite are the only clay minerals present within the kaolin deposit, associated with quartz, with small amounts of cristobalite, albite and hematite.

Propylitic alteration is quite widespread and surrounds the other alterations (Fig. 3). The alteration affects the volcanic rocks (andesite and rhyolite) and parts of the diorite porphyry and granodiorite porphyry and consists of chlorite, quartz, epidote, calcite and magnetite. A few traces of sericite are also present. The intensity of propylitic alteration varies from <10% to <50% in the host rocks. Primary plagioclase has been generally altered to calcite (3-5%) and epidote (5-

7%). In mafic mineral-bearing rocks (for example, biotite, amphibole, pyroxene), chlorite is abundant (15-20) together with epidote (2-3%), calcite (5-7%), sulfides (1-2%), and magnetite (1-3%) (Fig. 4d). Alteration is commonly weaker in the mafic rocks which lay farther from other rocks.

Wall rock alteration occurs as narrowly-developed zones around the mineralized vein and is composed of clay minerals, quartz and calcite, exhibiting argillic, silicification (Fig. 4e) and carbonitization (Fig. 4f). The argillic alteration is characterized by kaolinite and illite within wall rocks near the vein mineralization. Silicification occurs in wall rock as matrix with lesser amounts of kaolinite and calcite and the accompanied vein mineralization occurs as quartz–ore vein. In a distance from the vein, carbonitization alteration occurs as veins and veinlets. The mineral paragenesis at vein displays a progression from kaolinite–illite, through main-stage quartz, to late-stage calcite. The change from illite stability domain to that of calcite requires a corresponding evolution of the fluid to higher pH (e.g., Simmons and Christenson, 1994).

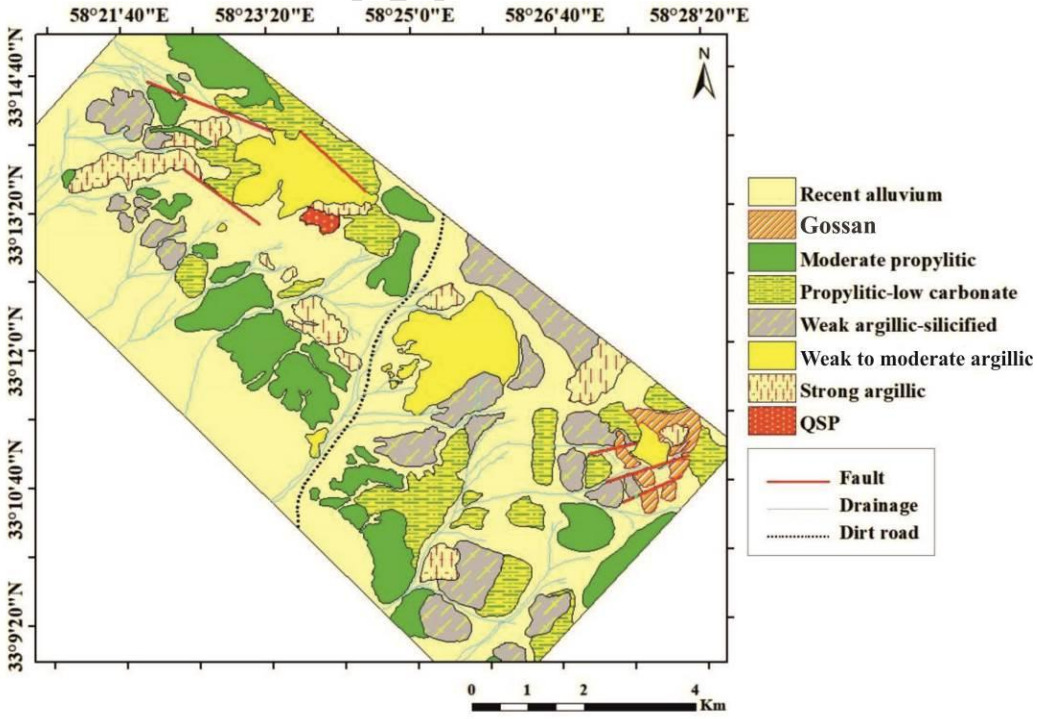

Fig. 3 Alteration map of Cheshmeh Khuri area.

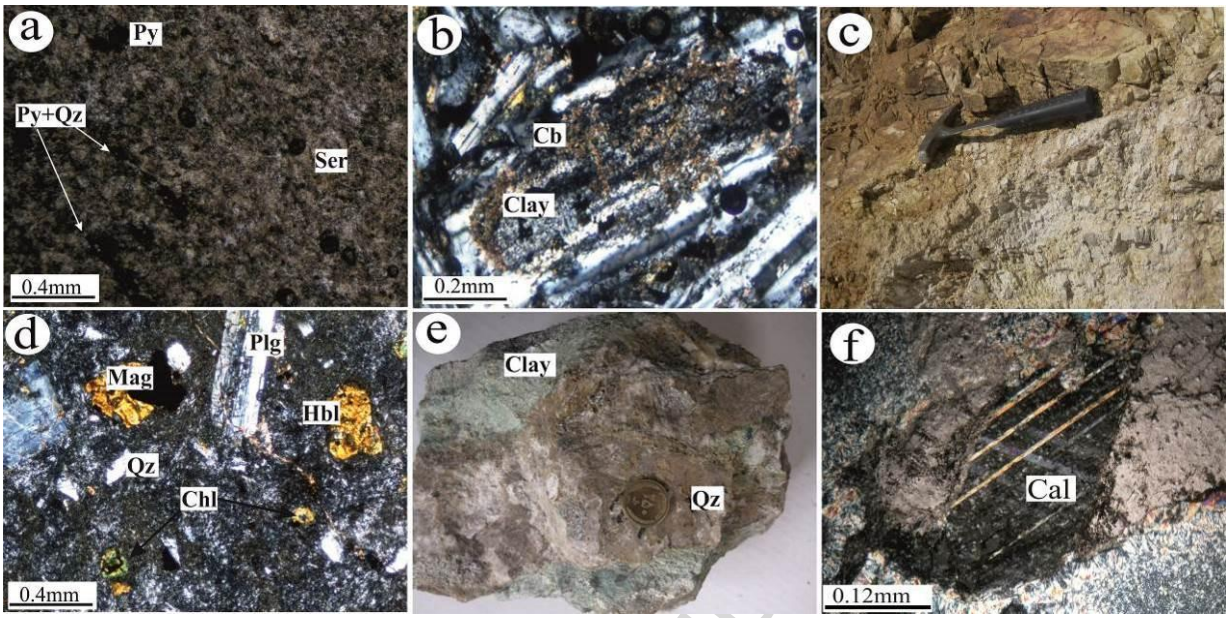

Fig. 4 Field photographs and photomicrographs of hydrothermal alteration assemblages in the Cheshmeh Khuri prospecting area: (a) Py+Qz veinlets in QSP±C zone, (b) replacement of plagioclase phenocryst by clay minerals and carbonate in moderate argillic zone, (c) kaolin deposit, (d) replacement of hornblende phenocrysts by chlorite and magnetite in propylitic zone, (e) argillic and silicification zones, (f) calcite in carbonitization zone of vein mineralization. Abbreviations: Py: Pyrite; Qz: Quartz; Cb: Carbonate; Chl: Chlorite; Cal: Calcite; Mag: Magnetite; Ser: sericite (Mineral abbreviations from Whitney and Evans, 2010).

6. Mineralization

The three main mineralization styles include stockwork, disseminated and vein. Based on polished and thin section studies, disseminated and stockwork mineralization types in QSP±C alteration consist of quartz, pyrite, carbonate, chalcopyrite and secondary minerals of chalcocite, covellite, jarosite, malachite and goethite (Fig. 6). Four types of veinlets (0.2mm–2cm thick) including quartz-calcite-pyrite±sericite, quartz-pyrite, quartz-chalcopyrite-pyrite (Fig. 5a) and

pyrite (Fig. 5b) are recognized in this alteration zone, whereas quartz-pyrite veinlets are the most abundant. The density of veinlets in the QSP alteration zone is ≤ 8 veinlets/m^2 at the surface. Pyrite is also as disseminated in this zone (Fig. 5c).

In the areas with propylitic alteration, disseminations and veinlets mineralization types contain pyrite, chalcopyrite, magnetite and secondary minerals (chalcocite, covellite, hematite and malachite). Based on their mineralogy, five types of veinlets (0.1-0.9mm thick) are recognized in this alteration type (pyrite-quartz-carbonate-chlorite, carbonate, quartz-carbonate-pyrite, quartz-magnetite-pyrite-carbonate (Fig. 5d) and carbonate-pyrite (Fig. 5e)), at which pyrite-quartz-carbonate-chlorite veinlets are the most abundant ones. Pyrite (5-7%) is the only sulfide ore mineral disseminated in the argillic zone, whereas strong argillic alteration with sulfides is not prevalent (Fig. 6).

Vein mineralization occurs in andesitic tuff breccia and along a fault zone trending northwest–southeast. Levorotation of the fault has caused a fracture system trending southwest (Fig. 2). Vein thickness considerably varies from 2 to 3 meters, whereas the strike can stretch up to 1 km. It cross-cuts the disseminated-style of mineralization. Microscopic studies reveal that the veins contain quartz, pyrite, chalcocite, tetrahedrite group (as inclusions) together with minor chalcopyrite, sphalerite and galena as hypogene minerals and chalcocite, digenite, covellite, malachite, atacamite, hematite, and goethite as supergene minerals. Quartz, calcite and barite are the dominant gangue minerals.

Chalcocite grains are large (Fig. 5f and g) and contain inclusions of chalcopyrite and tetrahedrite group (tetrahedrite–tennantite). Pyrite occurs as euhedral and/or subhedral grains in the vein (Fig. 5g) and less as disseminated in the host rock. Sphalerite mostly occurs as fine grains in the veins. Secondary chalcocite, covellite, digenite and malachite are mostly observed as overgrowth due to

formation of concentric textures along the borders and cracks of hypogene chalcocite and chalcopyrite (Fig. 5 h and i). Gossan has occurred as oxidized surface expressions of underlying ore zones. Minerals contain hematite, goethite, limonite and manganese oxides (The XRD was utilized in determining the minerals).

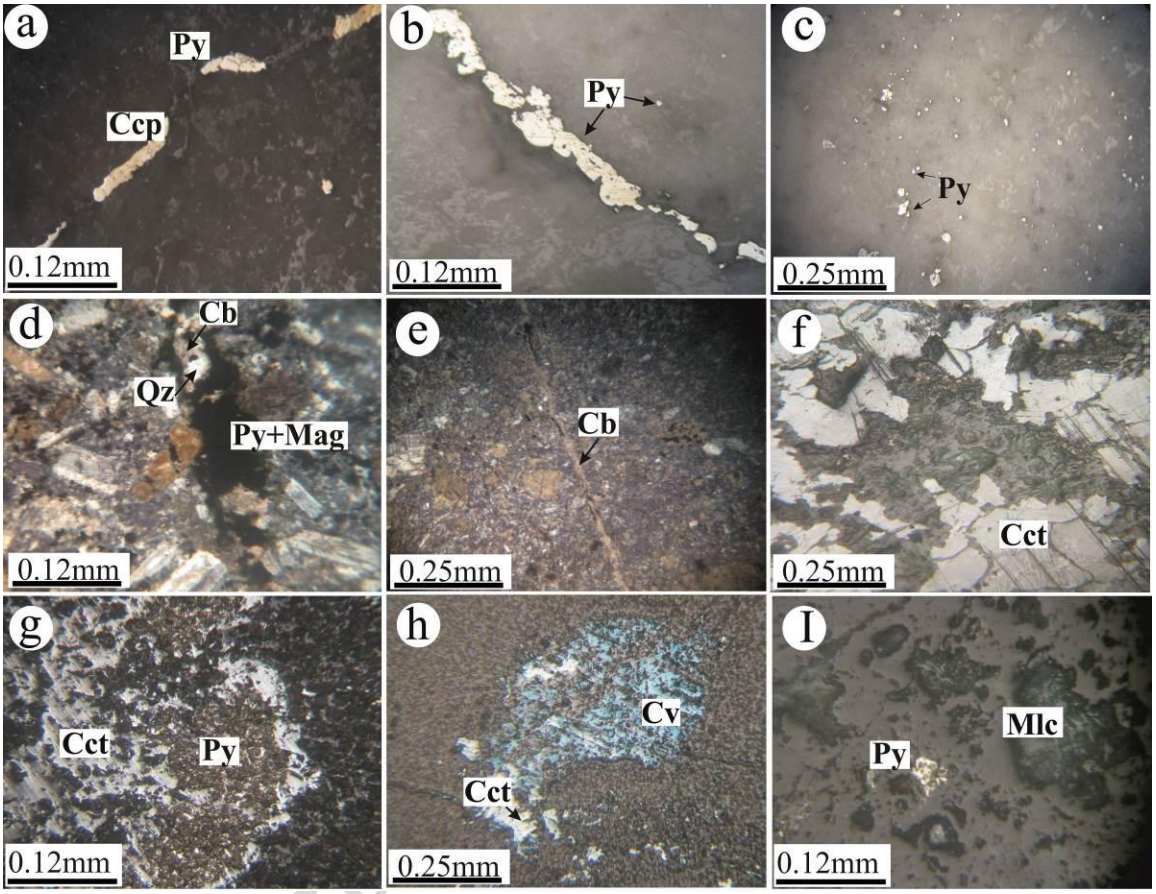

Fig. 5 Field photographs and photomicrographs of mineralization in the Cheshmeh Khuri prospecting area: (a) Py+Qz+Ccp veinlet, (b) Py veinlet, (c) disseminated pyrite in QSP±C zone, (d) Py+Mag+Qz+Cb veinlet in propylitic zone, Py+Cb veinlet in propylitic-carbonate zone, (f) chalcocite, (g) Py and Cc in hypogene vein mineralization, (h) chalcocite and covellite, (i) malachite in supergene zone. Abbreviations: Ccp: Chalcopyrite; Cct: Chalcocite; Cv: Covellite; Qz: Quartz; Cb: Carbonate; Py: Pyrite; Mag: Magnetite; Mlc: Malachite (Mineral abbreviations from Whitney and Evans, 2010).

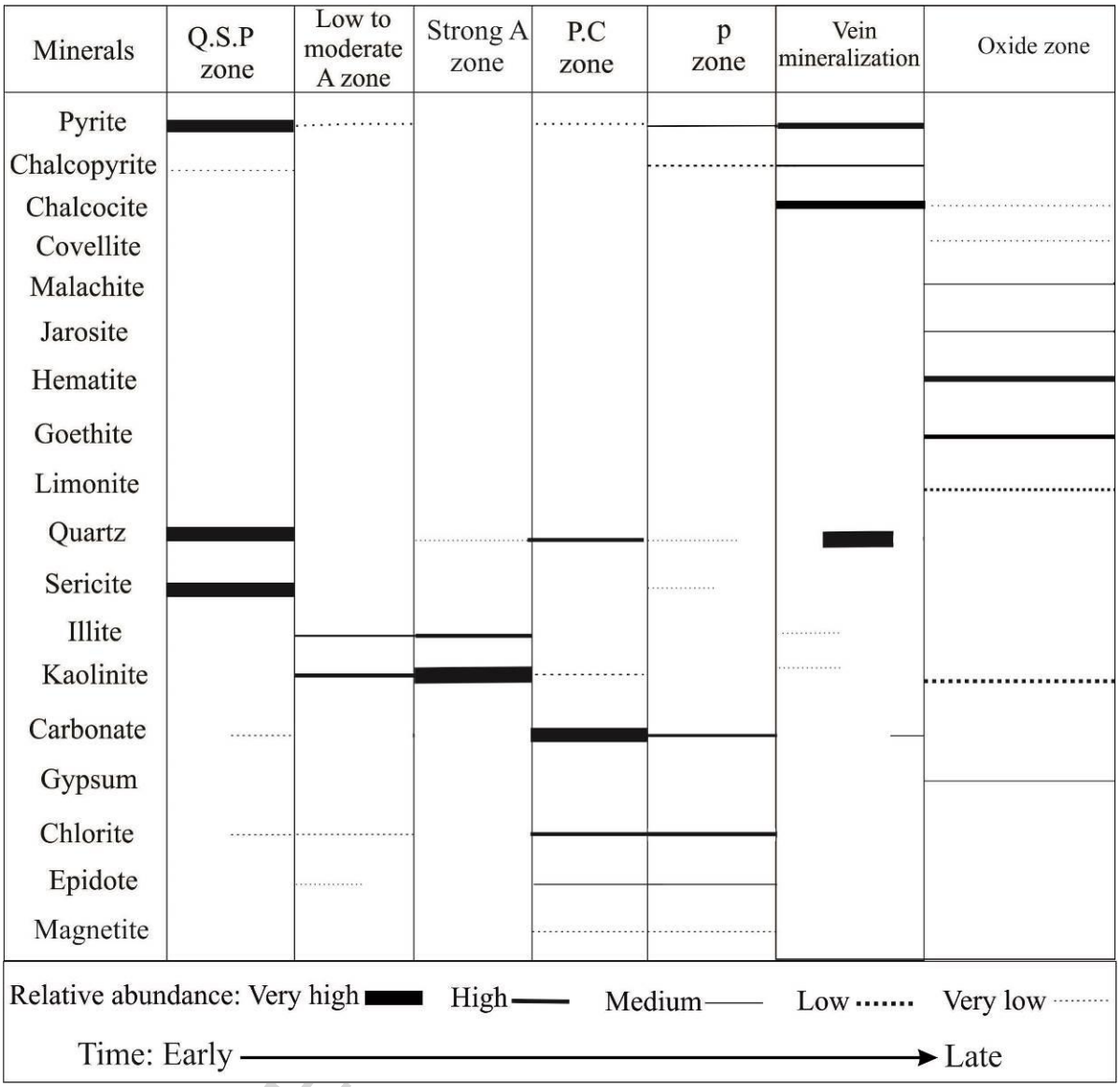

Fig. 6 Paragenetic mineral assemblages in the Cheshmeh Khuri area. Abbreviations: P: Propylitic, P.C: Propylitic-Carbonate, A: Argillic, Q.S.P±C: Quartz-Sericite-Pyrite±Carbonate.

7. Ore geochemistry

As can be seen in Table 1, Cu content reaches up to 654 ppm, 353 ppm and 5.07 % in QSP±C zone, propylitic and vein mineralization, respectively. The highest copper contents are closely associated with the QSP±C alteration zone (Cu=430–654 ppm, Mo=4-15 ppm, Zn=36-52 ppm

and Pb=13–162 ppm). Copper and molybdenum contents in propylitic alteration with disseminated mineralization (Cu=223-353 ppm, Mo=2-8 ppm, Zn=42-103 ppm, and Pb=21-1622 ppm) are lower than those in the QSP±C alteration zone.

Cu contents (1.14- 5.07 %) in vein-type mineralization originates from chalcopyrite and tetrahedrite group. Metal concentrations in some of the samples from the vein-type mineralization were Ag=4.4-16.3 ppm, As=18-105 ppm, Sb=15-27 ppm, Mo=3-5 ppm, Zn=36–165 ppm, and Pb=11-57 ppm. High As, Ag and Sb contents may have been originated from the tetrahedrite group: (tetrahedrite-tennantite). This is proven by high the correlation values among Sb–Ag (0.80), Sb–Cu (0.79) and Cu–Ag (0.95) pairs. Bi and gold contents are negligible in the three mineralization types.

Table 1. Results of ICP-OES analysis of ore samples from the Cheshmeh Khuri area.

Element	X	Y	Alteration	Mo (ppm)	Cu (ppm)	Sb (ppm)	Pb (ppm)	As (ppm)	Ag (ppm)	Au (ppb)	Zn (ppm)
CH-M1	58°25′27″E	33°10′41″N	P-C	-	223	-	21	-	-	-	56
CH-M2	58°23′60″E	33°13′8″N	QSP±C	7	573	-	13	-	1.3	17	52
CH-M3	58°23′42″E	33°13′18″N	QSP±C	6	430	-	47	-	-	6	36
CH-M4	58°23′37″E	33°13′22″N	QSP±C	5	652	-	162	-	4.7	15	48
CH-M5	58°22′49″E	33°13′9″N	P	4	348	-	201	-	-	-	76
CH-M6	58°22′52″E	33°12′20″N	P	2	321	-	230	-	-	-	84
CH-M7	58°22′19″E	33°14′8″N	P	8	312	-	672	14	-	4	53
CH-M8	58°22′21″E	33°14′30″N	P	5	353	-	79	13	-	-	64
CH-M9	58°24′46″E	33°12′42″N	P	5	332	-	19	-	-	-	95
CH-M10	58°23′34″E	33°13′27″N	QSP±C	15	566	-	17	-	2.4	7	38
CH-M11	58°23′34″E	33°12′29″N	PC	2	346	-	1622	-	-	-	42
CH-M12	58°24′28″E	33°13′3″N	PC	4	330	-	-	-	-	-	63
CH-M13	58°22′20″E	33°13′58″N	P	5	322	-	18	-	-	-	103
CH-M14	58°23′19″E	33°13′8″N	QSP±C	13	654	-	44	-	5.3	12	48

CH-M15	58°22′17″E	33°13′24″N	P	4	333	-	1314	-	-	-	98
V16	58°27′35″E	33°10′22″N	Vein	4	16600	15	57	34	9.3	-	154
V17	58°27′58″E	33°11′15″N	Vein	4	11400	27	44	86	4.4	-	127
V18	58°28′9″E	33°11′05″N	Vein	4	44200	24	24	105	16.3	-	165
V19	58°27′52″E	33°10′32″N	Vein	3	14000	16	15	25	5.9	-	57
V20	58°27′37″E	33°11′08″N	Vein	3	28700	18	15	44	8.0	-	36
V21	58°27′55″E	33°11′12″N	Vein	5	50700	16	11	18	11.1	-	78

(−) = below detection limit. Abbreviations: P: Propylitic, C: Carbonate, QSP: Quartz-Sericite-Pyrite.

8. Geochemistry of the igneous rocks

The results of major and trace element analyses for the Cheshmeh Khuri intrusive rocks are presented in Table 2. The Cheshmeh Khuri granitoid rocks have a range of SiO_2 contents from 57.95 to 67.08 wt% (Table 2) and mainly plot in the field of granodiorite and diorite of the Middlemost (1985) diagram (Fig. 7). In the K_2O vs. SiO_2 diagram (Peccerillo and Taylor, 1976), the granitoid samples define a trend in the field of the high-K calc-alkaline series (Fig. 8). In the diagram of A/NK vs. A/CNK (Maniar and Piccoli, 1989), the samples of granitoid rocks fall in the metaluminous field with A/CNK < 1.1 (molar Al_2O_3/ ($CaO + K_2O + Na_2O$)) (Fig. 9).

The mafic rocks plot in the field of gabbro, gabbrodiorite and monzodiorite and belong to the high-K calc-alkaline series in the K_2O vs. SiO_2 diagram, except for two samples which fall in the field of the shoshonite series (Figs. 7 and 8).

Table 2. Whole-rock major and trace element compositions of the studied intrusive rocks of Cheshmeh Khuri area.

Sample	CH46	CH56	CH4	CH14	CH39	CH30	P26
X	58°22′5″E	58°22′12″E	58°25′26″E	58°25′6″E	58°23′59″E	58°23′51″E	58°26′57″E
Y	33°12′13″N	33°14′20″N	33°9′19″N	33°11′3″N	33°13′21″N	33°10′57″N	33°10′47″N
Type	Di ph	Di ph	Gr ph	Gr ph	Gr ph	Mzd ph	Di ph
				Wt. %			
SiO_2	62.34	56.95	66.07	62.45	67.08	53.90	61.44
TiO_2	0.68	0.73	0.48	0.62	0.34	0.86	0.72
Al_2O_3	14.94	14.85	16.27	14.50	15.72	15.08	16.04
FeOt	5.09	5.69	3.73	4.46	3.10	7.52	5.87
MnO	0.09	0.10	0.04	0.08	0.05	0.11	0.14
MgO	3.28	5.14	1.11	3.80	1.36	5.45	1.41
CaO	4.42	5.80	3.17	4.47	2.19	8.08	5.71
Na_2O	2.83	2.76	3.50	2.99	2.99	2.88	4.23
K_2O	3.40	2.85	3.37	3.56	3.50	3.12	2.84
P_2O_5	0.21	0.21	0.21	0.33	0.16	0.37	0.25
LOI	1.91	3.83	1.37	1.85	0.94	2.10	1.15
Total	99.76	99.54	99.74	99.61	99.78	99.47	99.8
				ppm			
Ba	647	1097	475	917	880	1802	380
Be	1	<1	<1	1	1	4	<1
Co	16.30	21.60	5.10	16.90	1.80	26.70	13.50
Cs	3.10	2.10	3.30	1.90	2.60	1.10	17.30
Ga	16	17.20	17.30	14	16.30	16	15.50
Hf	5	3.40	4.50	3.90	4.80	3.60	4.20
Nb	9.80	7.80	7.30	7.30	11.50	7.80	7.70
Rb	117	75.80	90.40	104	114	65.90	47.30
Sn	1	1	2	<1	<1	1	<1
Sr	645	1911	442	907	663	2614	576
Ta	0.70	0.50	0.50	0.50	0.70	0.50	0.70
Th	14.30	13.30	8.70	12.50	12.10	28.70	7.10
U	4.30	3.70	2.80	4.30	3.70	5.20	2
V	143	154	44	128	31	260	114
W	2.10	1.10	1.30	0.80	1.60	1.20	0.90
Zr	183	134	161	142	198	135	165
Y	19.40	14.80	11	14.20	13.20	18.30	19.70
La	31.80	45.10	26.20	27.50	34.80	79	21.60
Ce	64	82.20	52.20	50.50	64.10	152.40	41.20
Pr	7.07	9.27	5.78	5.60	6.53	17.19	4.71
Nd	27.30	32.70	21.40	21.30	22.20	65.90	18.20
Sm	5.27	5.42	4.09	3.90	3.85	10.25	3.58
Eu	1.17	1.38	0.95	0.97	0.86	2.34	1.07
Gd	4.49	4.09	3.43	3.29	3.13	6.69	3.64
Tb	0.66	0.53	0.46	0.46	0.41	0.77	0.59
Dy	3.63	2.93	2.28	2.54	2.39	4.19	3.28
Er	2.21	1.57	1.07	1.50	1.37	1.96	2.11

Tm	0.34	0.24	0.16	0.22	0.21	0.30	0.32
Yb	2.16	1.58	1.02	1.35	1.53	1.94	2.24
Lu	0.31	0.24	0.15	0.22	0.25	0.28	0.35
			Ratios				
*Eu/Eu	0.73	0.89	0.77	0.83	0.76	0.86	0.91
$(La/Yb)_N$	9.93	19.24	17.32	13.73	15.33	27.45	6.50

Table 2 *(continued)*

Sample	CH20	CH22	P15	P17	CH35	P25	P37
Longitude	58°24′29″E	58°24′16″E	58°27′31″E	58°27′20″E	58°24′9″E	58°26′53″E	58°27′28″E
Latitude	33°13′12″N	33°13′4″N	33°10′32″N	33°10′39″N	33°12′5″N	33°10′48″N	33°11′8″N
Petrography	Di ph	Di ph	G	G	Gd ph	Gd ph	G
			Wt. %				
SiO_2	61.17	59.21	48.13	48.81	55.14	52.09	48.99
TiO_2	0.62	0.59	1.18	1.15	1.00	1.21	1.15
Al_2O_3	15.02	15.07	16.36	18.24	16.57	18.50	17.87
FeOt	4.81	5.41	9.18	9.12	8.01	8.74	8.94
MnO	0.07	0.08	0.18	0.18	0.15	0.12	0.16
MgO	4.11	4.80	6.83	5.46	5.03	1.73	5.60
CaO	4.75	5.02	10.71	10.11	7.31	9.12	9.75
Na_2O	3.17	2.71	2.59	2.80	2.86	3.63	2.73
K_2O	2.89	2.73	1.85	1.72	2.11	1.82	1.49
P_2O_5	0.15	0.16	0.46	0.38	0.21	0.36	0.36
LOI	2.51	3.99	1.35	0.84	0.52	0.89	1.80
Total	99.80	99.77	99.84	99.82	99.80	99.18	99.84
			ppm				
Ba	684	651	240	254	329	367	232
Be	1	3	<1	<1	<1	2	<1
Co	15	14.40	37.60	34.20	29.10	14.40	32.30
Cs	1.6	3	2	1.50	3	3.30	1.40
Ga	16.40	14.80	14.10	16.40	16.10	16.70	17
Hf	3.70	3.50	2.30	2.40	3	2.80	2.50
Nb	9	7.80	3.10	3.40	6.10	3.90	3
Rb	83.60	86.30	36.30	37.10	59.90	59.10	32.60
Sn	1	<1	<1	1	<1	<1	<1
Sr	634	660	435	528	528	537	520
Ta	0.70	0.60	0.10	0.20	0.50	0.20	0.20
Th	8.30	7.90	3.40	3.50	5.70	4.50	3.50
U	2.40	2.80	0.90	0.70	1.60	2.50	0.90
V	116	93	300	285	247	406	288
W	0.70	1.90	<0.5	0.50	0.70	8.90	<0.5
Zr	136	134	82.0	85.8	111	105	97.8
Y	12	13.30	22.50	22.50	21.10	26.50	24.10
La	21.40	22.90	13.30	14.20	18.70	24.10	14.20
Ce	40.20	44.20	27.80	29.50	41.20	40.60	30.70
Pr	4.30	4.78	3.56	3.80	5.01	4.57	3.88
Nd	14.90	19	15.90	16.80	22	19.80	16.90
Sm	2.83	3.21	3.78	4.09	4.62	4.53	4.18

Eu	0.84	0.84	1.15	1.31	1.30	1.38	1.40
Gd	2.70	2.60	4.21	3.96	4.40	4.82	4.70
Tb	0.43	0.42	0.70	0.67	0.71	0.81	0.78
Dy	2.38	2.49	4.02	4.07	4.11	4.83	4.66
Er	1.69	1.52	2.54	2.50	2.40	3.16	2.93
Tm	0.21	0.19	0.37	0.37	0.37	0.44	0.41
Yb	1.50	1.38	2.41	2.46	2.41	2.84	2.85
Lu	0.21	0.21	0.35	0.35	0.37	0.45	0.44
			Ratios				
*Eu/Eu	0.93	0.89	0.88	0.99	0.88	0.90	0.97
$(La/Yb)_N$	9.61	11.19	3.72	3.89	5.23	5.72	3.36

Abbreviations: G: Gabbro, Gd ph: Gabbrodiorite porphyry, Mzd ph: Monzodiorite porphyry, Di ph: Diorite porphyry, Gr ph: Granodiorite porphyry, LOI: Loss On Ignition.

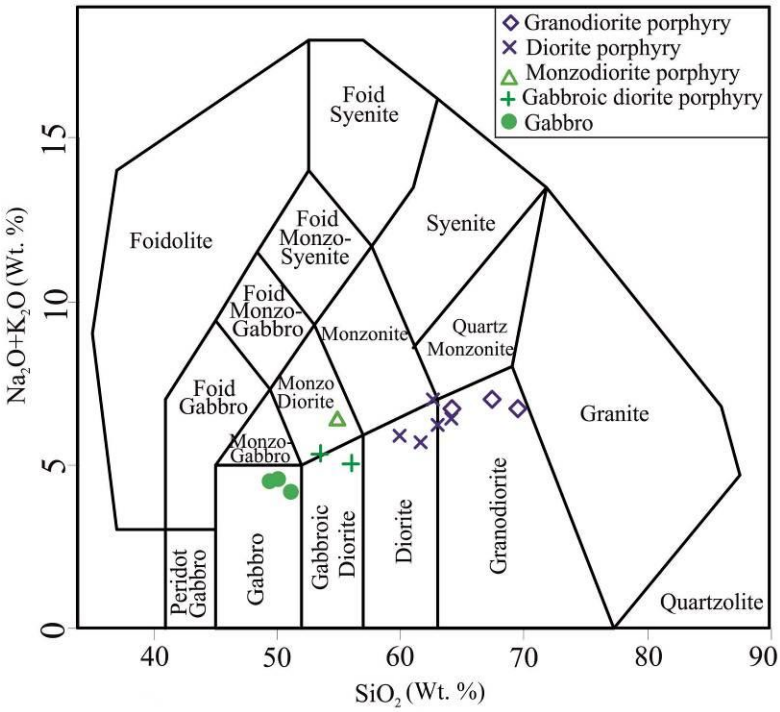

Fig. 7 Classification of intrusive rocks in $Na_2O+ K_2O$ vs. SiO_2 TAS diagram (Middlemost, 1985).

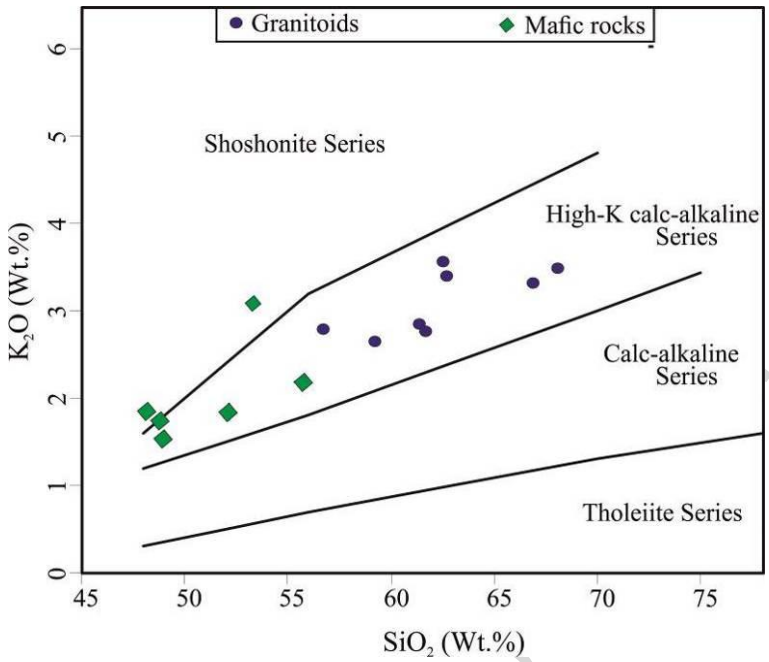

Fig. 8 Intrusive rocks in K_2O vs. SiO_2 diagram (Peccerillo and Taylor, 1976).

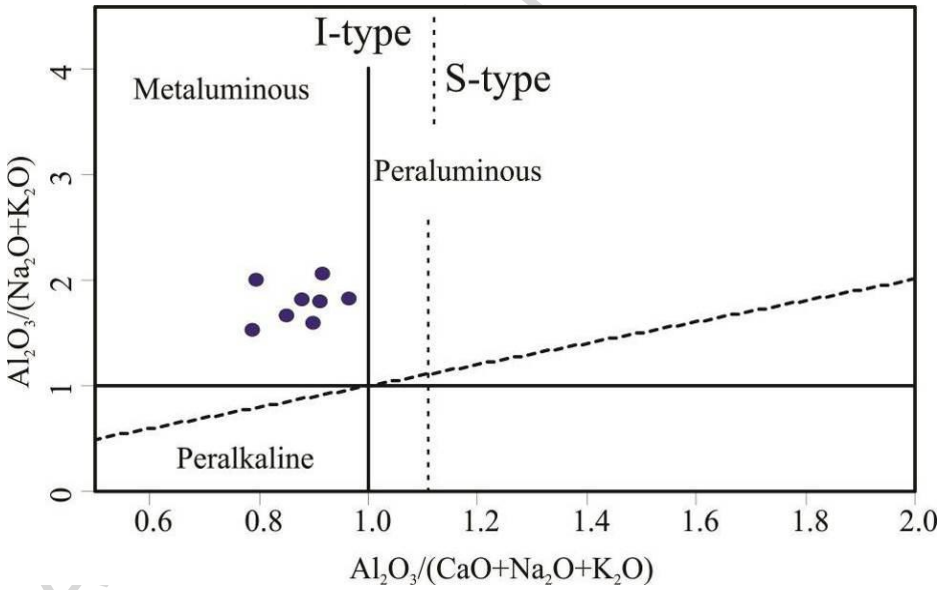

Fig. 9 Subvolcanic rocks in $Al_2O_3/Na_2O + K_2O$ (molar) vs. $Al_2O_3/(CaO + K_2O + Na_2O)$ diagram (molar) (Maniar and Piccoli, 1989) and the field boundaries between S-type and I-type granite are from Chappell and White (1992).

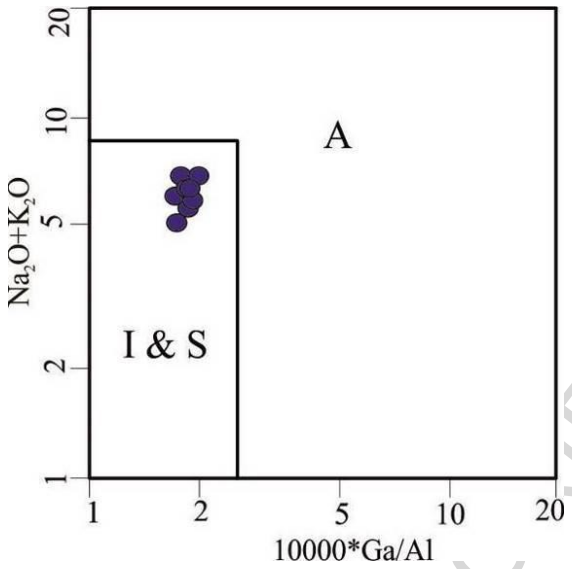

Fig. 10 I and S from A-type granitoids discrimination diagram for the Cheshmeh Khuri rocks (Whalen et al., 1987).

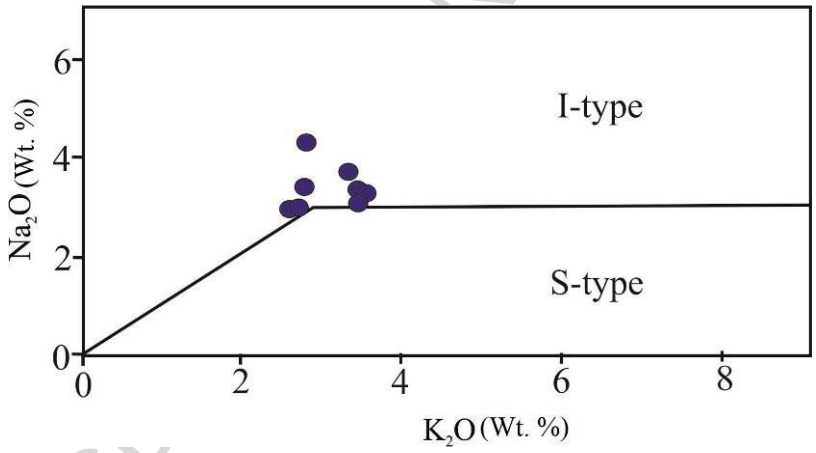

Fig. 11 Discrimination diagram for I and S-type granitoids by %Na_2O vs. %K_2O (Chappell and White, 2001). Boundary between I and S-types is Na_2O = 3%.

In the plots of 10,000 Ga/Al vs. (K_2O +Na_2O) (Whalen et al., 1987), the granitoid samples fall in the fields of I- and S-type granites (Fig. 10). Moreover, the samples in a Na_2O vs. K_2O diagram (Fig. 11, Chappell and White, 2001) are consistent with the I-type character of granitoid rocks.

In the chondrite normalized REE diagram (Boynton, 1984), the granitoid samples show patterns with medium to slightly strong LREE enrichment ($6.5 \leq La_N/Yb_N \geq 19.2$) (Fig. 12a). Negligible negative Eu anomalies are noted for granitoid samples (0.73 to 0.93) (Table 2).

The chondrite-normalized REE patterns for mafic rocks are non-parallel. The mafic rocks (except monzodiorite porphyry) show weak heavy rare earth element (HREE) depletion and low fractionation between LREE and HREE (La_N/Yb_N =3.3–5.7) (Fig. 12c). These ratios are lower than those in the magmas (>20 e.g., Martin, 1987) whose source contains garnet. The REE pattern for the monzodiorite porphyry is completely different (La_N/Yb_N=27.4) (Fig. 12c) and suggests the presence of garnet in the residual (Wilson, 1989; Rollinson, 1993).

In the primitive mantle-normalized trace element spider diagrams (Sun and McDonough, 1989), the granitoid samples display strong enrichments in large-ion lithophile elements (LILE), such as Rb, Ba, Cs and K and other incompatible elements that behave similar to those of LILE (Th and U). When compared to LILE, the most characteristic high-field strength elements (HFSE: Nb, Zr, Y, and Ti) clearly indicate lower normalized values; Nb, Ti systematically display strong negative anomalies (Fig. 12b). The mafic rocks show weaker negative anomalies for P and Ti, although they are only slight in the most mafic compositions, or even absent for P in the gabbro compositions (Fig. 12d).

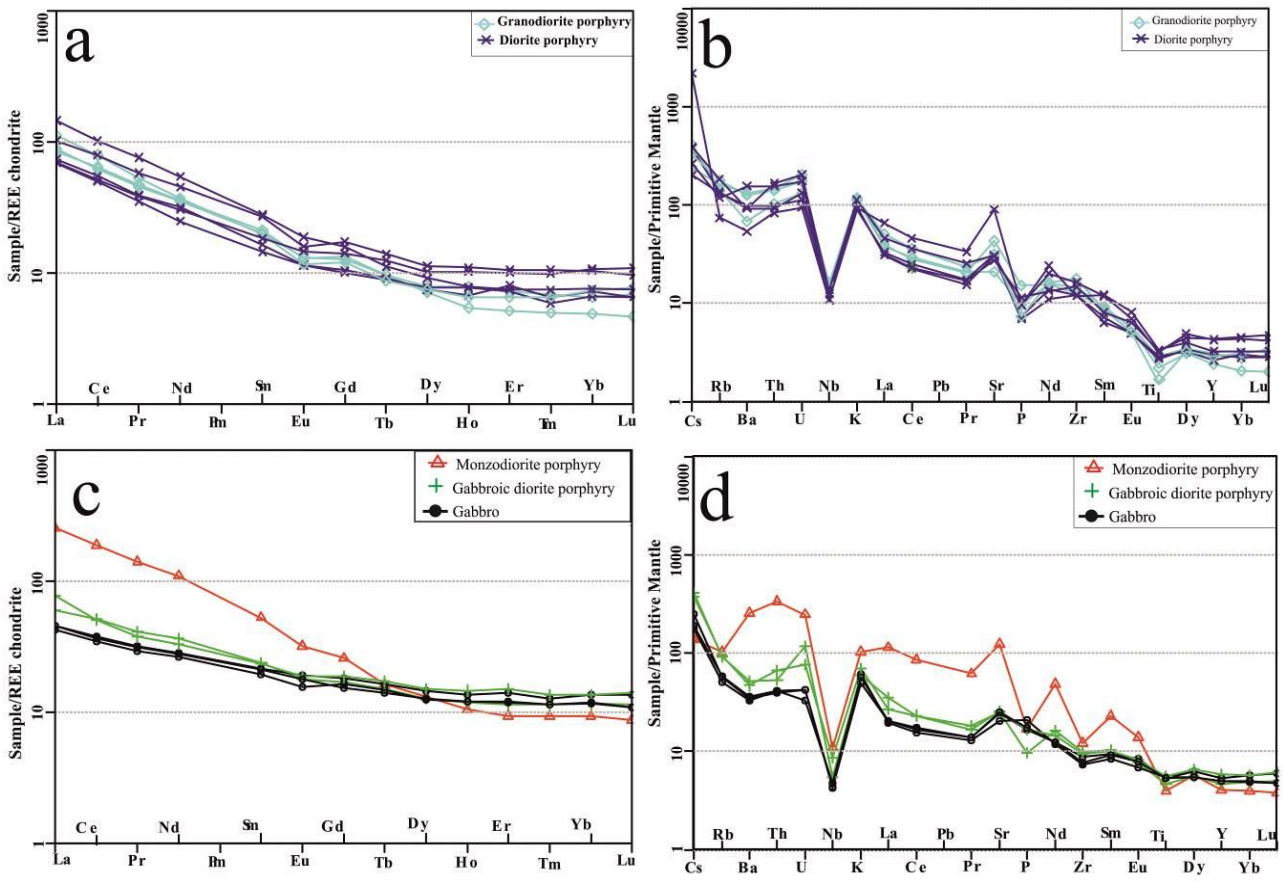

Fig. 12 Chondrite-normalized rare earth elements and Primitive mantle-normalized trace element for the Cheshmeh Khuri granitoid and mafic rocks.

9. Magnetic susceptibility

Granitoids with magnetic susceptibility of value over $>50\times10^{-5}$ (SI units), are classified as belong to the magnetite series (Ishihara, 1981). Measurements of magnetic susceptibility for the rock types are shown in Fig. 13. Different amounts of the magnetic susceptibility of granitoids are related to the effect of the hydrothermal alteration on these units (e.g., Lang et al., 2013; Shah et al., 2013).

The low susceptibility ranges of altered granitoids have been consistent with the hydrothermal destruction of igneous magnetite during argillic and QSP±C alterations. In contrast, the high

susceptibility ranges of altered granitoids have been consistent with the generation of magnetite during of the propylitic alteration. Magnetic susceptibility for fresh granitoids is mostly high values (750×10^{-5} SI to 3200×10^{-5} SI) which is indicative of magnetite series.

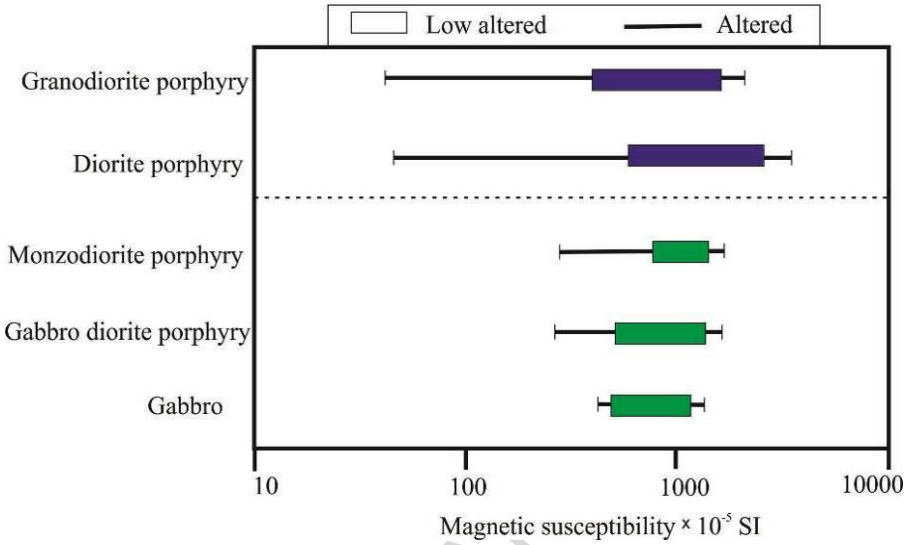

Fig. 13 Magnetic susceptibility vs. rock types.

10. Rb–Sr and Sm–Nd isotope geology

There is a close relationship between granitoids and mineralization in the Cheshmeh Khuri area. Therefore, two of the least altered samples (granodiorite porphyry (CH14) and diorite porphyry (CH20)) were selected for Rb–Sr mineral–whole-rock dating with the objective of obtaining geochronological information on the magmatic events associated with mineralization.

Biotite, hornblende and plagioclase concentrates were obtained from the CH20 sample and, together with the whole-rock analysis, the $^{87}Sr/^{86}Sr$ and $^{87}Rb/^{86}Sr$ ratios define a line whose slope corresponds to an age of 43.4 ± 3.2 Ma (MSWD = 25) (Fig. 14) and to an initial $^{87}Sr/^{86}Sr$ = 0.70522. Since the plagioclase, hornblende and whole-rock data plot close to each other, the result is strongly dependent on the Sr isotopic composition of biotite. Therefore, it should be

mainly viewed as a biotite Rb–Sr age. The MSWD age was calculated according to model 3 of Ludwig (2012). In order to date the CH14 sample, hornblende, plagioclase and whole rock compositions were used. The result was a 44.6 ± 5.4 Ma isochron (Fig. 15), with MSWD = 3.0 and initial $^{87}Sr/^{86}Sr$ = 0.70476, obtained by following the model 1 of Ludwig (2012).

Taking into consideration that the Cheshmeh Khuri granitoids were emplaced in a shallow crustal level (sub-volcanic), their post-emplacement cooling should have been fast. Therefore, the 43-45 Ma age (Middle Eocene) may be viewed as dating of the magmatic event.

The initial $^{87}Sr/^{86}Sr$ and $^{143}Nd/^{144}Nd$ for intrusive rocks of the Cheshmeh Khuri are calculated at 44 Ma based on their average age (Table 3). The granitoid rocks display a narrow variability in initial $(^{87}Sr/^{86}Sr)_i$ ratios, ranging from 0.7047 to 0.7054, and εNd_i values of -1.1 to +0.8. According to Chappell and White (1974), the values of $(^{87}Sr/^{86}Sr)_i$ below 0.708 are characteristic of I-type granitoids. The mafic rocks display variability in initial $(^{87}Sr/^{86}Sr)_i$ ratios, 0.7043 for gabbro and 0.7047 for monzodiorite porphyry, and have εNd_i values +3.5 for the gabbro and +0.7 for the monzodiorite. In the εNd_i versus $(^{87}Sr/^{86}Sr)_i$ diagram, all samples plot slightly to the right of the so-called mantle array (Fig. 16).

Table 3. Rb–Sr and Sm–Nd isotopic data from six whole-rock samples, two plagioclase separate, two hornblende and one biotite separate from the Cheshmeh Khuri area.

Sample	Sr (ppm)	Rb (ppm	$^{87}Rb/^{86}Sr$	Error (2s)	$^{87}Sr/^{86}Sr$	Error (2s)	$(^{87}Sr/^{86}Sr)_i$	Nd (ppm)	Sm (ppm	$^{147}Sm/^{144}Nd$	Error (2s)	$(^{143}Nd/^{144}Nd)_m$	Error (2s)	εNd_i
CH14	907	104	0.333	0.009	0.704973	0.000017	0.70476	21.30	3.90	0.111	0.006	0.512655	0.000015	+0.8
CH14-P	2073	6.37	0.0089	0.0003	0.704776	0.000018								
CH14-H	297	9.47	0.0922	0.0026	0.704799	0.000028								
CH20	634	83.60	0.381	0.011	0.705387	0.000021	0.70515	14.90	2.83	0.115	0.006	0.512558	0.000021	-1.1
CH20-P	1308	22.50	0.0497	0.0014	0.705305	0.000025								
CH20-B	65.90	295	12.95	0.37	0.713083	0.000034								
CH20-H	175	15.10	0.249	0.007	0.705373	0.000018								
CH39	663	114	0.498	0.014	0.705798	0.000017	0.70549	22.20	3.90	0.105	0.006	0.512558	0.000014	-1.0
CH46	645	117	0.524	0.015	0.705423	0.000023	0.70510	27.30	5.27	0.117	0.006	0.512564	0.000012	-1.0
CH30	2614	65.9	0.073	0.002	0.704747	0.000018	0.70470	65.90	10.05	0.092	0.003	0.512645	0.000021	+0.7
P17	529	37.10	0.203	0.006	0.704503	0.000038	0.70438	16.80	4.09	0.147	0.008	0.512803	0.000016	+3.5

Note: The initial ratio of $^{87}Sr/^{86}Sr$ for each sample, calculated using $^{87}Rb/^{86}Sr$ and $(^{87}Sr/^{86}Sr)m$ and an age of 44 Ma (the age based on Rb–Sr isochron). The initial ratio of $^{143}Nd/^{144}Nd$ for each sample, calculated using $^{147}Sm/^{144}Nd$ and $(^{143}Nd/^{144}Nd)m$ and an 44 Ma (the age based on Rb–Sr isochron). CH20B, CH20H and CH20P represent biotite, hornblende and plagioclase separates of sample CH20, respectively. CH14P and CH14H represent plagioclase and hornblende separates of sample CH14, respectively.

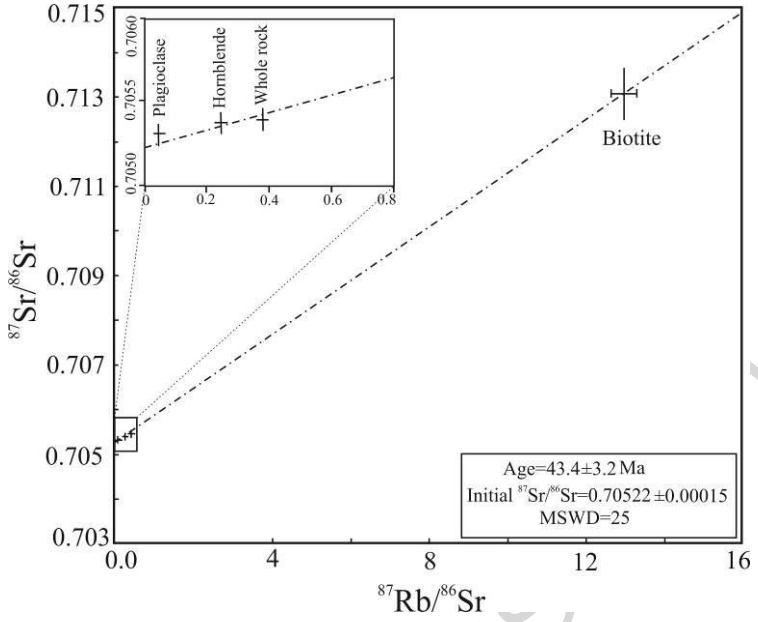

Fig. 14 Plot of the whole rock-plagioclase- hornblende -biotite isochron of diorite porphyry (CH20).

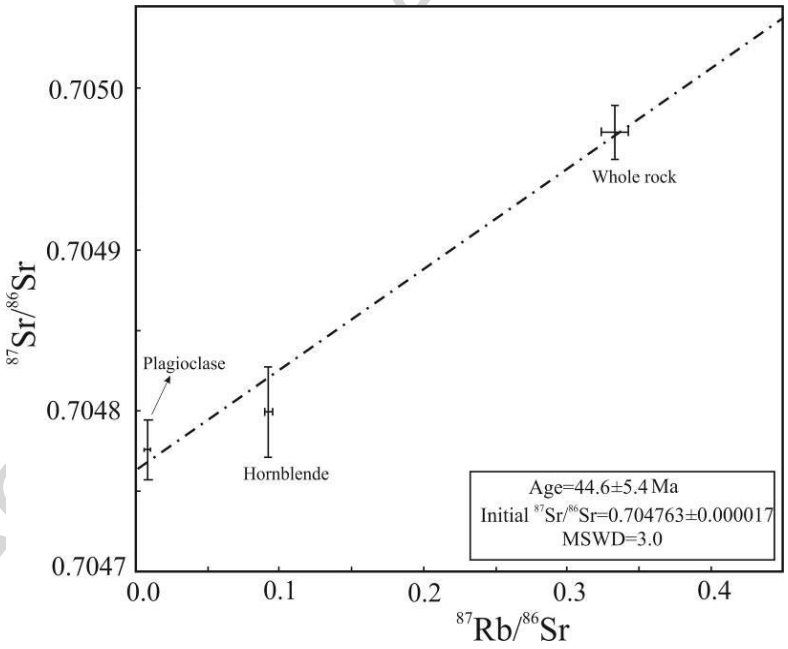

Fig. 15 Plot of the whole rock-plagioclase-hornblende isochron of granodiorite porphyry (CH14).

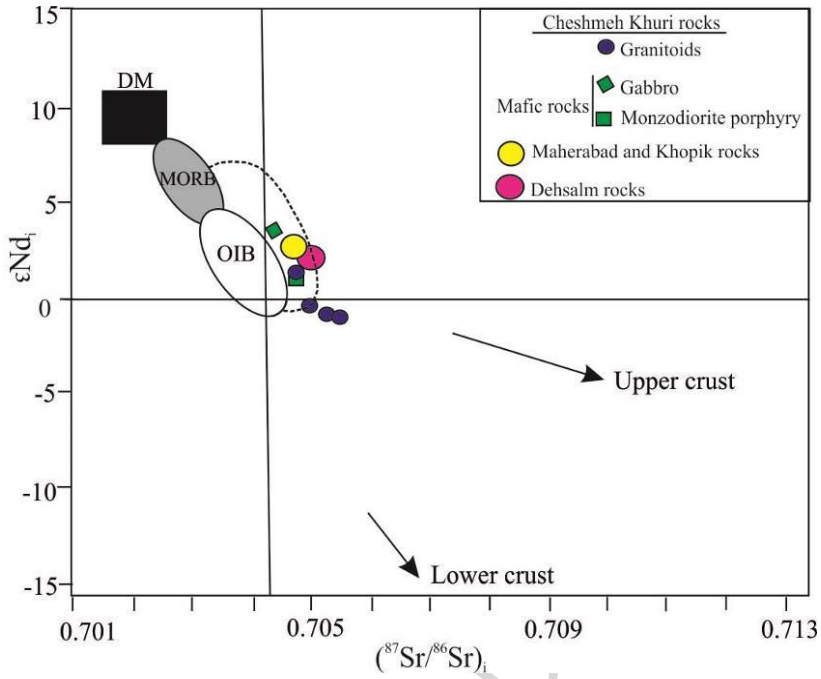

Fig. 16 εNd_i vs. $(^{87}Sr/^{86}Sr)_i$ diagram for the Cheshmeh Khuri rocks. Reference data sources: upper continental crust (Taylor and McLennan, 1985); lower continental crust (Rollinson, 1993; Rudnick, 1995) with those of MORB (Rollinson, 1993; Sun and McDonough, 1989), DM (McCulloch and Bennett, 1994), OIB (Vervoort et al., 1999), IAB (Arjmandzadeh and Santos, 2014). MORB: Mid-ocean ridge basalts; DM: Depleted mantle; OIB: Ocean-island basalts; IAB: island-arc basalts.

11. U–Pb zircon age determination results

In order to confirm Rb-Sr dating, we also performed U–Pb dating on diorite porphyry (CH20). U–Pb data are listed in Table 4. Zircons from the diorite porphyry show euhedral–subhedral shapes and typical oscillatory growth zoning. The U/Th ratios are lower than 5 (1.1 to 1.9 with an average of 1.5), and are in agreement with magmatic zircons (Table 4).

According to zircon U–Pb data, diorite porphyry show the Eocene age of 43.7±0.5 Ma (n=8, MSWD=4.5) (Fig. 17a and b); while some inherited cores yielded older ages of 543.0±13 Ma

(n=6, MSWD=10.7) (Fig. 17c). U–Pb analyses of zircons with inherited cores from the Cheshmeh Khuri area suggest that the crust of the Lut Block might not be entirely juvenile (Neoproterozoic) and have the potential presence of continental fragments with Gondwanan affiliation.

Table 4. Summary of zircon U–Pb ages of diorite porphyry (CH20).

Analysis	U (ppm)	$^{206}Pb/^{204}Pb$	U/Th	$^{206}Pb/^{207}Pb$	± (%)	$^{207}Pb/^{235}U$	± (%)	$^{206}Pb/^{238}U$	± (%)	Best age	± (Ma)
1	220	1522	1.8	24.5957	12.3	0.0381	12.8	0.0066	3.4	42.5	1.5
2	215	1512	1.8	21.2881	2.9	0.0451	4.1	0.0067	3.1	43.6	1.3
3	159	46625	1.2	19.6838	2.5	0.0464	3.9	0.0065	3.0	42.6	1.3
4	1130	18579	1.1	21.2615	1.4	0.0441	6.3	0.0068	6.1	43.7	2.7
5	181	2668	1.9	21.2727	5.6	0.0436	6.2	0.0067	2.7	43.2	1.2
6	388	9276	1.2	21.2866	2.5	0.0451	4.2	0.0068	3.3	44.7	1.4
7	273	11152	1.5	21.0204	2.6	0.0451	3.9	0.0070	2.8	44.2	1.3
8	139	2258	1.6	21.4451	1.9	0.0437	3.3	0.0068	2.6	43.7	1.2
9	328	50451	2.0	16.9808	1.2	0.6683	1.2	0.0823	3.9	510.1	19.2
10	695	191152	3.9	17.4131	1.3	0.6738	1.3	0.0851	2.7	526.7	13.8
11	256	33818	6.1	17.2354	0.9	0.6843	0.9	0.0856	3.0	529.4	15.3
12	429	74547	1.7	17.0064	1.1	0.7168	1.1	0.0885	2.9	546.4	15.0
13	344	126885	3.7	16.7294	1.2	0.7404	1.2	0.0899	2.6	554.8	13.6
14	149	35674	6.9	16.4931	1.2	0.7776	1.2	0.0931	2.5	573.6	13.9
15	83	23512	3.4	14.6140	1.2	1.3403	1.2	0.1421	2.2	856.6	17.6

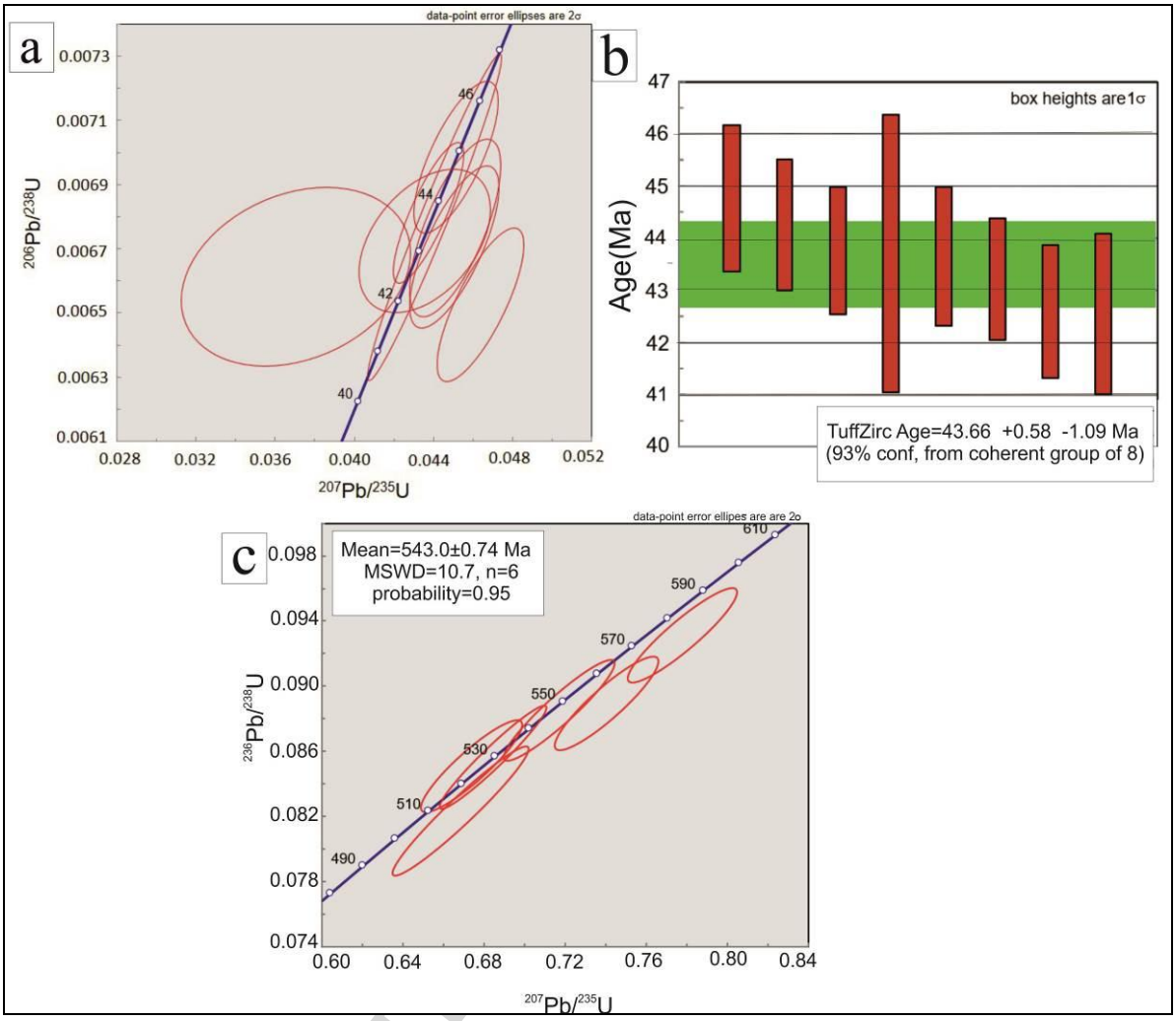

Fig. 17 a) the Concordia diagram, b) the average age plot for magmatic zircons and c) the Concordia diagram for inherited cores of diorite porphyry (CH20).

12. Discussion

12.1. The AFC processes or partial melting

The recorded small variation in isotopic ratios can be related either to variable crustal assimilation (but always in small degrees) or to heterogeneity in the magma source (Nabatian et al., 2014). Variation trends of εNd_i and $(^{87}Sr/^{86}Sr)_i$ of granitoid rocks are in agreement with

crustal assimilation (Fig. 18). In contrast, variation in isotopic ratios of mafic rocks may be related to heterogeneity in the magma source.

Negative εNd_i values display the features of the crustal melt, and the positive εNd_i isotopic ratios are consistent with mantle array (Kemp et al., 2007; Li et al., 2009; Yang et al., 2007). On the diagram of the εNd_i vs. $(^{87}Sr/^{86}Sr)_i$, the granitoid samples display a trend toward the upper continental crust, implying that the crust contamination has played a role in magma evolution. In contrast, mafic rocks do not show evidence for contamination with continental crust (Fig. 16). In granitoid rocks, the mantle component was subsequently modified by crustal contamination and assimilation as evidenced by the presence of inherited zircons.

In the diagram of the compatible elements vs. incompatible elements, the granitoid and mafic compositions are consistent with a partial melting trend and lack any compositional variation indicative of fractional crystallization (Fig. 19). Hence, we may conclude that partial melting has played an important role during the magmatic evolution of the granitoid and mafic rocks.

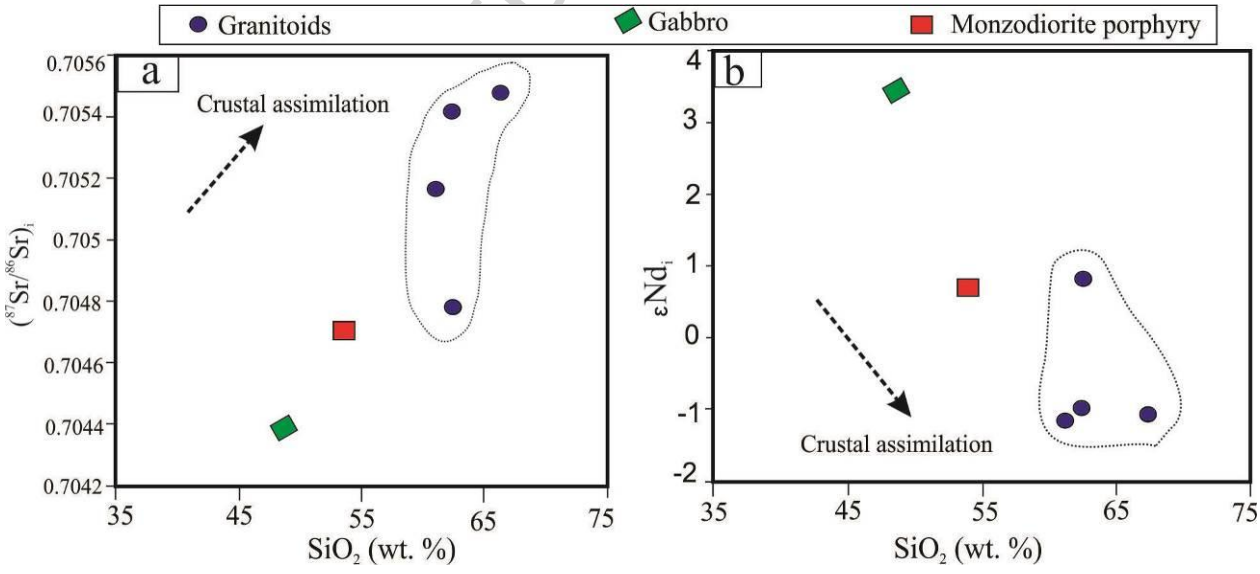

Fig. 18 $(^{87}Sr/^{86}Sr)_i$ ratios and εNdi values vs. SiO_2 diagrams (Xu et al., 2014) for the Cheshmeh Khuri samples.

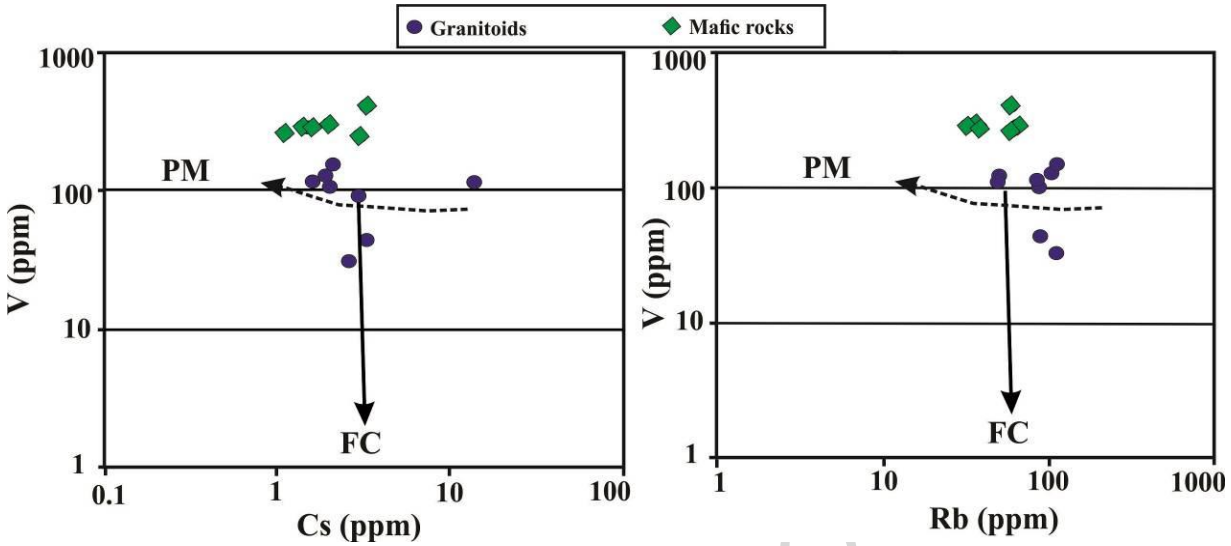

Fig. 19 Diagrams of the compatible elements versus incompatible elements for the Cheshmeh Khuri samples.

12.2. Residual phases and magma sources

The studied rocks have no obvious negative Eu (granitoid samples: 0.73 to 0.93 and mafic samples: 0.86 to 0.99) (Table 2). The normal content of the Eu may possibly be due to a lack of or low content of plagioclase or high oxygen fugacity in the source (Martin, 1999) and/or minimal fractionation of this mineral in the early crystallization stages (Best, 2003). The presence of H_2O in the melts may possibly decrease the pressure and temperature conditions of formation of plagioclase and increase the crystallization field of amphibole (Gill, 1981; Green, 1982).

Middle to slightly strong LREE enrichment for granitoids ($6.5 \leq La_N/Yb_N \geq 19.2$) and weaker heavy rare earth element (HREE) depletion (for mafic rocks (La_N/Yb_N =3.3–5.7: gabbros and gabbrodiorites) are lower than those in the magmas (>20 e.g., Martin, 1987) whose source contain garnet. Amphibole can substantially fractionate middle LREE/HREE ratio (Rollinson, 1993). Therefore, amphibolite is the most likely source for the parental magmas of the granitoids

and mafic rocks. High depletion in HREE (La_N/Yb_N=27.4) ratio for the monzodiorite porphyry suggests presence of garnet in the residual (Rollinson, 1993; Wilson, 1989). A source with the presence of garnet and absence of plagioclase is generally thought to occur at depths > 40 km (or >1.2 GPa) (Petford and Atherton, 1996; Rapp and Watson, 1995; Xu et al., 2014).

12.3. Petrogenesis

The most obvious trace element characteristics of rocks in the study area are negative Nb, Zr, and Ti anomalies and positive Sr, K, Rb and Ba anomalies, in addition to highly enriched LREE patterns, all showing the signature of a mantle source metasomatized by the slab-derived fluid/melt. The lower LILE and LREE of magmas from mafic rocks propose greater interaction within the mantle of slab-derived melts (e.g., Stern and Kilian, 1996).

High Sr and low Nb, Ta and Ti contents are thought to be developed due to the absence of plagioclase and presence of Fe–Ti oxides in the residue in the source area of the parental magmas (Martin, 1999). Negative Nb anomalies are also characteristic of the continental crust and, in many cases, they are probably related with processes of assimilation, contamination or mixing with crustal materials (Asran and Ezzat, 2012; Ma et al., 2014; Rollinson, 1993; Wilson, 1989; Zhang et al., 2006). The phosphorus negative anomalies in the studied samples can be explained by fractionation of apatite.

However, the diagram of Nb/Yb vs. Th/Yb shows that all of the samples from the plot above the MORB–OIB array (Pearce and Peate, 1995), obviously indicate a subduction component in their sources (Fig. 20). The position of the studied samples to the right of the mantle array (Fig. 16) might have been related to an origin of the most primitive magmas by melting in a supra-subduction mantle wedge (Stolz et al. 1996).

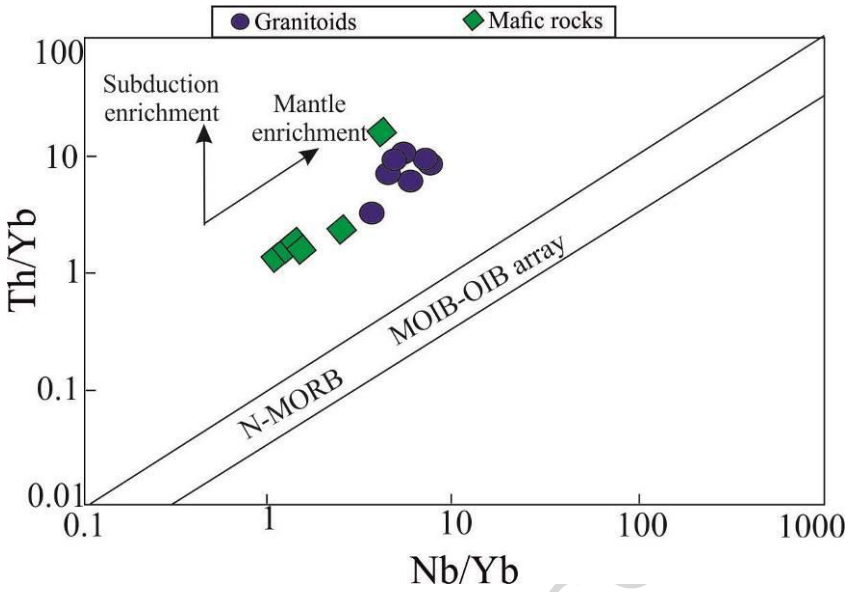

Fig. 20 Th/Yb vs. Nb/Yb plot showing the relation of the granitoid and mafic rocks from the Cheshmeh Khuri area and the MOB–OIB array of Pearce and Peate (1995).

12.4. Tectonic setting

In the Th vs. Ta diagram from Schandl and Gorton (2002), all the samples of the Cheshmeh Khuri prospect area plot in the field of active continental margins (Fig. 21). In order to determine the tectonic setting of granitoids from the study area, the tectonic discrimination diagrams of Pearce et al. (1984) were used. All granitoid samples are plotted in the volcanic arc granites (I-type) field (Fig. 22).

The extended exposure of Eocene–Oligocene volcanic and intrusive rocks is the special characteristic of the Lut Block. These rocks cover half of the Lut Block with a thickness of 2000 m (Berberian et al., 1999; Camp and Griffis, 1982; Tirrul et al., 1983). The time of existence and closure mechanisms of the Sistan Ocean are not well constrained yet. The age for ocean closure and thus the Lut–Afghan collision was considered by some researcher to be in the Late Cretaceous (Angiboust et al., 2013; Zarrinkoub et al., 2012). In contrast, several authors (e.g.,

Arjmandzadeh et al, 2011; Camp and Griffis, 1982; Arjmandzadeh and Santos, 2014; Tirrul et al., 1983) suggest that the closure of the Sistan Ocean and Lut–Afghan continental blocks collision did not take place before Eocene.

The Sistan Ocean existed at least from the Early Cretaceous (Babazadeh and de Wever, 2004) between the Lut and Afghan continental blocks. Zircon U–Pb ages of 113 ± 1 and 107 ± 1 Ma in two leucogabbros of the Birjand ophiolite indicate that this part of the Sistan Ocean has been opened by Mid-Cretaceous (Zarrinkoub et al., 2012). Bröcker et al. (2013) dated samples of different metamorphic grades and geographic locations in the ophiolitic belt and concluded that subduction was active in the Late Cretaceous (from ca. 83 to 87 Ma ago). According to the emplacement ages of ~86–71 Ma on adakitic plutons and ~55 Ma on A-type granites in the suture zone, the Lut and Afghan blocks collided in the Late Cretaceous (Zarrinkoub et al., 2010).

Pang et al. (2013) proposed that the magmatism was caused by convective removal of the lithosphere and the resultant asthenospheric upwelling during extensional collapse of the east Iranian ranges in the Eocene–Oligocene time. In such a setting, lithospheric mantle is expected to be slightly influenced by slab-derived material. So, metasomatism of the lithospheric mantle beneath must be related to an ancient subduction event (during the Late Cretaceous Sistan subduction).

We determined an I-type affinity for the granitoid rocks in the Cheshmeh Khuri according to the conventional granitoid classification schemes (Fig. 10, Fig 11 and Fig 22). According to new data about subduction in the Late Cretaceous, the Middle Eocene granitoids could not be categorized through a purely subduction-related magmatism. So, the parental melts of these rocks have originated from a subduction-modified upper mantle in the post-collisional extension-related zone.

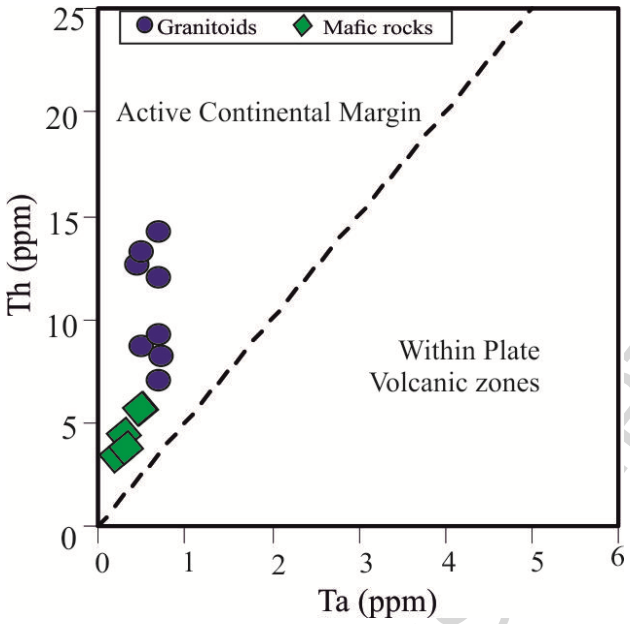

Fig. 21 Tectonomagmatic discrimination diagram for the Cheshmeh Khuri rocks (Schandl and Gorton, 2002).

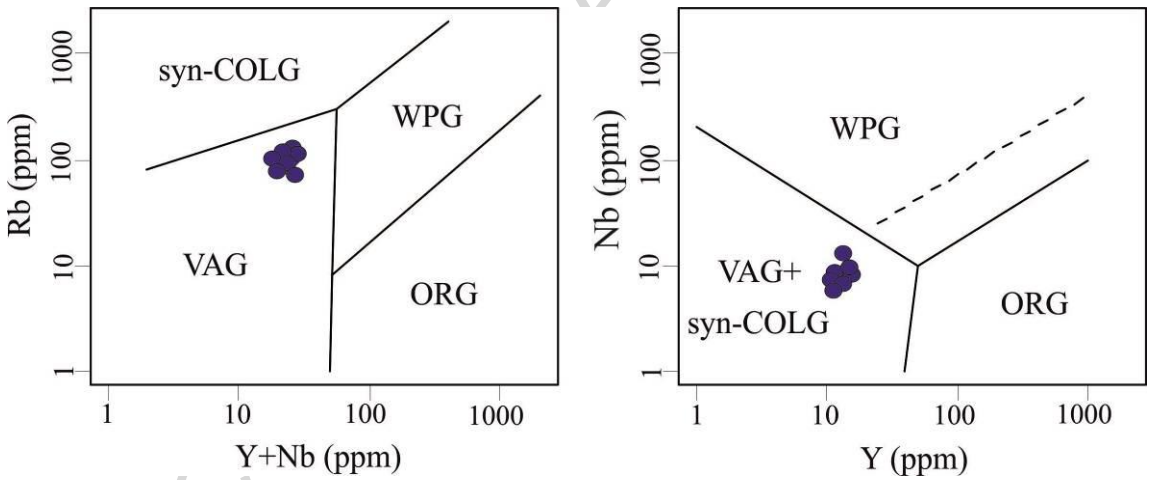

Fig. 22 Tectonomagmatic discrimination diagrams for the Cheshmeh Khuri rocks (Pearce et al., 1984), (a) Nb+Y vs. Rb and (b) Y vs. Nb. WPG, within plate granites; VAG, volcanic arc granites; ORG, ocean ridge granites; syn-COLG, syncollisional granites.

12.5 Mineralization in the Cheshmeh Khuri prospect

Copper mineralization at the Cheshmeh Khuri prospect area is spatially and temporally associated with magnetite-series of oxidized, granitoids (granodiorite porphyry and diorite porphyry). Wall rock alterations associated with Cu mineralization are similar to a porphyry system, including quartz-sericite-pyrite±carbonate, argillic and propylitic. Porphyry-style of mineralization is characterized by disseminations and stockworks. The Cheshmeh Khuri prospect is suggested to represent a porphyry system formed in the post-orogenic extension-related magmatism. The copper vein-type mineralization clearly post-dates porphyry-style mineralization by noting the cross-cutting relationship between them.

A number of base metal vein deposits have superimposed on the porphyry copper deposits (e.g., Baumgartner and Fontboté, 2008; Bendezú et al., 2003), whereas others have no known link to the mineralized porphyry deposits (Einaudi et al., 2003). Numerous Cu±Ag±Zn±Pb veins are present in the neighboring areas (Shikasteh Sabz, Mire-e-Khash, Rashidi, Shurk, Ghar-e-Kaftar and Howz-e-Dagh, Chah Khareh, and Chang-e-Namakzar veins; Lotfi, 1982; Javidi Moghaddam et al., 2018). The similarities in ore mineralogy and geochemistry may point out that all these veins are part of a regional ore system (Javidi Moghaddam et al., 2018) and may, therefore these veins be related to a porphyry copper system. This scenario (the relationship between these veins and porphyry copper mineralization in the Cheshmeh Khuri area) needs more studies on fluid evolution, magma source and the genetic type in both types of mineralization.

12.6. Geochemical differences among the Cu Porphyry districts in the Lut Block

The location of major Tertiary Cu porphyry mineralization occurrences within the Lut Block is shown in Fig. 1. Intrusive rocks related to copper porphyry deposits of the Lut Block are high-K to shoshonitic and calc-alkaline (Khopik, Maherabad and Cheshmeh Khuri; Malekzadeh Shafaroudi, 2009) to adakitic affinity (Dehsalm; Arjmandzadeh and Santos, 2014). These rocks

originated from partial melting in a subduction-modified upper mantle. Cu and Au are chalcophile elements that are highly compatible in mantle rocks within sulfide phases (Ballard et al., 2002; Fleet et al., 1996). The granitoid samples of Cheshmeh Khuri show slightly lower εNd_i values than the Khopik, Maherabad and Dehsalm samples, indicating that those of the granitoid samples should have experienced less mantle interaction than that of the Khopik, Maherabad and Dehsalm samples. It is proposed that the Cheshmeh Khuri district has the lowest potential for a significant amount of Cu–Au accumulation because the mantle is an important supply for these metals.

13. Conclusion

Zones of argillic and marginal propylitic alteration have surrounded a QSP±C alteration assemblage. Copper mineralization was localized in stockwork veinlets (with high Cu anomalies) and disseminated grains in the adjacent altered rock matrix. Patterns of hydrothermal alteration assemblages and mineralization styles have similarities with porphyry copper deposits systems. Cu vein mineralization has occurred in the peripheral to porphyry copper mineralization, crosscutting porphyry-style mineralization, and may have formed later in the evolution of the porphyry system.

The variety of geochemical and isotopic patterns of granitoid and mafic rocks illustrates the different roles of magma sources, partial melting, fractional crystallization, crustal assimilation and crustal contamination in post-collisional extension zone. The Middle Eocene granitoids of the Cheshmeh Khuri district are primarily high-K calc-alkaline, metaluminous and are classified as belong to the magnetite-series of oxidized granitoids.

A comparison of the geochemical and isotopic data of Cu mineralization districts in the Lut Block suggests that granitoids of the Cheshmeh Khuri district have originated from partial

melting in a subduction-modified upper mantle, followed by a relatively small crustal interaction. In contrast, other granitoids (Khopik, Maherabad and Dehsalm) also have the same petrogenesis. However, they have slightly higher amounts of mantle materials with no evidence of interaction with the crust. Therefore, it may be conclude that the Cheshmeh Khuri granitoids have a lower potential for Cu–Au mineralization than that of the Khopik, Maherabad and Dehsalm districts.

Acknowledgments

The Research Foundation of Ferdowsi University of Mashhad, Iran, supported this study (Project No. 22731.3). The authors wish to thank Mrs. Sara Ribeiro (Laboratório de Geologia Isotópica da Universidade de Aveiro) for the TIMS analysis process and for the guidance and assistance during sample preparation in the clean room. Sr and Nd isotope analyses financially supported the Portuguese Foundation for Science and Technology, through project Geobiotec (UID/GEO/04035/2013).

References

Aghazadeh, M., Hou, Z., Badrzadeh, Z., Zhou, L., 2015. Temporal–spatial distribution and tectonic setting of porphyry copper deposits in Iran: Constraints from zircon U–Pb and molybdenite Re–Os geochronology. Ore Geology Review 70, 385–406.

Angiboust, S., Agard, P., De Hoog, J.C.M., Omrani, J., Plunder, A., 2013. Insights on deep, accretionary subduction processes from the Sistan ophiolitic “melange” (Eastern Iran). Lithos 156, 139–158.

Arjmandzadeh, R., Karimpour, M.H., Mazaheri, S.A., Santos, J.F., Medina, J., Homam, S.M., 2011. Sr–Nd isotope geochemistry and petrogenesis of the Chah-Shaljami granitoids (Lut Block, Eastern Iran). Asian Earth Sciences 41 (3), 283–296.

Arjmandzadeh, R., Santos, J.F., 2014. Sr–Nd isotope geochemistry and tectonomagmatic setting of the Dehsalm Cu–Mo porphyry mineralizing intrusives from Lut Block, eastern Iran. International Journal of Earth Sciences (Geologische Rundschau) 103 (1), 123–140.

Asran, M., Ezzat, M., 2012. The pan-African calc-alkaline granitoids and the associated mafic microgranular enclaves (MME) around Wadi Abu Zawal area, North Eastern desert, Egypt: geology, geochemistry and petrogenesis. Biology and Earth Sciences 2 (1), 1–16.

Babazadeh, S.A., de Wever, P., 2004. Early Cretaceous radiolarian assemblages from radiolarites in the Sistan Suture (eastern Iran). Geodiversitas 26 (2), 185–206.

Ballard, J.R., Palin, J.M., Campbell, I.H., 2002. Relative oxidation states of magmas inferred from Ce (IV)/Ce (III) in zircon: application to porphyry copper deposits of northern Chile. Contributions to Mineralogy and Petrology 144 (3), 347–364.

Baumgartner, R., Fontboté, L., 2008. Mineral Zoning and Geochemistry of Epithermal Polymetallic Zn-Pb-Ag-Cu-Bi Mineralization at Cerro de Pasco. Peru Economic Geology 103 (3): 493–537.

Bendezú, R., Fontboté, L., Cosca, M., 2003. Relative age of Cordilleran base metal lode and replacement deposits, and high-sulfidation Au-(Ag) epithermal mineralization in the Colquijirca mining district, central Peru. Mineralium Deposita 38 (6), 683–694.

Berberian, M., Jackson, J.A., Qorashi, M., Khatib, M.M., Priestley, K., Talebian, M., Ghafuri-Ashtiani, M., 1999. The 1997 may 10 Zirkuh (Qaenat) earthquake (Mw 7.2): faulting along the Sistan suture zone of eastern Iran. Geophysical Journal International 136 (3), 671–694.

Berberian, M., King, G.C.P., 1981. Towards a paleogeography and tectonic evolution of Iran. Canadian Journal of Earth Sciences 18 (2), 210–265.

Best, M.G., 2003. Igneous and Metamorphic Petrology: Turin, Blackwell Publishing, p. 729.

Boynton, W.V., 1984. Geochemistry of the rare earth elements: meteorite studies, In: Henderson, P. (Ed.), Rare Earth Element Geochemistry. Elsevier, Amsterdam, pp. 63–114.

Bröcker, M., Fotoohi Rad, G., Burgess, R., Theunissen, S., Paderin, I., Rodionov, N., Salimi, Z., 2013. New age constraints for the geodynamic evolution of the Sistan Suture Zone, eastern Iran. Lithos 170, 17–34.

Camp, V.E., Griffis, R.J., 1982. Character, genesis and tectonic setting of igneous rocks in the Sistan suture zone, eastern Iran. Lithos 15 (3), 221–239.

Chappell, B.J., White, A.J.R., 1974. Two contrasting granite types. Pacific Geology 8, 173– 174.

Chappell, B.W., White, A.J.R., 1992. I- and S- type granites in the Lachlan fold belt, transactions of the royal society of Edinburg. Earth Sciences 83, 1–26.

Chappell, B.W., White, A.J.R., 2001. Two contrasting granite type: 25 years later. Australian Journal of Earth Sciences 48 (4), 489–499.

Einaudi, M.T., Hedenquist, J.W., Inan, E., 2003. Sulfidation state of hydrothermal fluids: The porphyry-epithermal transition and beyond. Society of Economic Geologists and Geochemical Society Special Publication 10, 285–313.

Fleet, M.E., Crocket, J.H., Stone, W.E., 1996. Partitioning of platinum group elements (Os, Ir, Ru, Pt, Pd) and gold between sulfide liquid and basalt melt. Geochimica et Cosmochimica Acta 60, 2397–2412.

Gehrels, G.E., Valencia, V.A., Ruiz, J., 2008. Enhanced precision, accuracy, efficiency, and spatial resolution of U–Pb ages by laser ablation-multicollector-inductively coupled plasma-mass spectrometry. Geochemistry, Geophysics, Geosystems 9, 13.

Gill, J.B., 1981. Orogenic Andesites and Plate Tectonics. Springer, New York.

Green, T.H., 1982. Anatexis of mafic crust and pressure crystallization of andesite, In: Thorpe, R. S. (Ed.), Andesites: Orogenic andesites and related rocks: Chicester, John Wiley & Sons, pp. 465-487.

Hezarkhani, A., Williams-Jones, A.E., Gammons, C.H., 1999. Factors controlling copper solubility and chalcopyrite deposition in the Sungun porphyry copper deposit. Mineralium Deposita. 34, 770–783.

Ishihara, S., 1981. The granitoid series and mineralization. Economic Geology 75, 458–484.

Jamali, H., Dilek, Y., Daliran, F., Yaghubpur, A., Mehrabi, B., 2010. Metallogeny and tectonic evolution of the Cenozoic Ahar-Arasbaran volcanic belt, northern Iran. International Geology Review 53, 608–630.

Javidi Moghaddam, M., Karimpour, M.H., Ebrahimi Nasrabadi, K., Haidarian Shahri, M.R., Malekzadeh Shafaroudi, A., 2018. Mineralogy, Geochemistry, Fluid Inclusion and Oxygen Isotope Investigations of Epithermal Cu ± Ag Veins of the Khur Area, Lut Block, Eastern Iran. Acta Geologica Sinica, in press.

Karimpour, M.H., Malekzadeh Shafaroudi, A., Stern, C.R., Farmer, L., 2012. Petrogenesis of Granitoids, U-Pb zircon geochronology, Sr-Nd isotopic characteristic, and important occurrence of Tertiary mineralization within the Lut Block, eastern Iran. Iranian Journal of Economic Geology 4, 1–27.

Karimpour, M.H., Stern, C.R., 2009. Advance spaceborne thermal emission and reflection radiometer (ASTER) mineral mapping to discriminate high sulfidation, reduced intrusion related, and iron oxide gold deposits, eastern Iran. Applied Sciences 9, 815–825.

Kemp, A.I.S., Hawkesworth, C.J., Foster, G.L., Paterson, B.A., Woodhead, J.D., Hergt, J.M., Gray, C.M., Whitehouse, M.J., 2007. Magmatic and crustal differentiation history of granitic rocks from hafnium and oxygen isotopes in zircon. Science. 315, 980–983.

Lang, J.R., Gregory, M.J., Rebagliati, C.M., Payne, J.G., Oliver, J.L., Roberts, K., 2013. Geology and magmatic-hydrothermal evolution of the giant Pebble porphyry copper-gold-molybdenum deposit, southwest Alaska, USA. Economic Geology 108 (3), 437–462.

Li, X.H., Li, W.X., Wang, X.C., Li, Q.L., Liu, Y., Tang, G.Q., 2009. Role of mantle-derived magma in genesis of early Yanshanian granites in the Nanling Range, South China: in situ zircon Hf–O isotopic constraints. Sciences China, Series D Earth Sciences 52 (9), 1262-1278.

Lotfi, M., 1982. Geological and geochemical investigations on the volcanogenic Cu, Pb, Zn, Sb ore-mineralization in the Shurab-Gale Chah and northwest of Khur (Lut, east of Iran). Unpublished Ph.D thesis, der Naturwissenschaften der Universitat Hamburg.

Lotfi, M., 1995. Geological map of Iran sheet 7756 (Birjand), scale 1:100,000, Geological Survey of Iran, Tehran (in Persian).

Ludwig, K.R., 2012. Isoplot 3.75: A Geochronological Toolkit for Microsoft Excel. Berkeley Geochronology Center Special Publication 5, 75 pp.

Ma, L., Jiang, S., Hou, M., Dai, B., Jiang, Y., Yang, T., Zhao, K., Wie, P., Zhu, Z., Xu, B., 2014. Geochemistry of early cretaceous calc-alkaline lamprophyres in the Jiaodong Peninsula: Implication for lithospheric evolution of the eastern North China craton. Gondwana Research 25, 859–872.

Maghsoudi, A., Yazdi, M., Mehrpartou, M., Vosoughi, M., Younesi, S., 2014. Porphyry Cu– Au mineralization in the Mirkuh Ali Mirza magmatic complex, NW Iran. Asian Earth Science 79, 932–941.

Malekzadeh Shafaroudi, A., 2009. Geology, mineralization, alteration, geochemistry, microthermometry, isotope studies and determining the mineralization source of Khopic and Maherabad exploration areas. Ph.D thesis. Ferdowsi university of Mashhad.

Malekzadeh Shafaroudi, A., Karimpour, M.H., Stern, C.R., 2015. The Khopik porphyry copper prospect, Lut Block, Eastern Iran: Geology, alteration and mineralization, fluid inclusion, and oxygen isotope studies. Ore geology Reviews 65 (2), 522–544.

Maniar, P.D., Piccoli, P.M., 1989. Tectonic discrimination of granitoids. Geological Society of America Bulletin 101 (5), 635–643.

Martin, H., 1987. Petrogenesis of Archaean trondhjemites, tonalites and granodiorites from eastern Finland: major and trace element geochemistry. Petrology 28, 921–953.

Martin, H., 1999. The adakitic magmas: modern analogues of Archaean granitoids. Lithos 46 (3), 411–429.

McCulloch, M.T., Bennett, V.C., 1994. Progressive growth of the Earth's continental crust and depleted mantle: Geochemical constraints. Geochimica et Cosmochimica Acta 58, 4717–4738.

McInnes, B.I.A., Evans, N.J., Fu, F.Q., Garwin, S., Belousova, E., Griffin, W.L., Bertens, A., Sukama, D., Permanadewi, S., Andrew, R.L., Deckart, K., 2005. Thermal history analysis of selected Chilean, Indonesian, and Iranian porphyry Cu–Mo–Au deposits, In: Porter, T.M. (Ed.), Supper Porphyry Copper and Gold Deposits: A Global Perspective. PGC publishing, Adelaide, pp. 1–16.

Middlemost, E.A.K., 1985. Magmas and Magmatic Rocks, Longman, London & New York.

Mirnejad, H., Mathur, R., Hassanzadeh, J., Shafie, B., Nourali, S., 2013. Linking Cu mineralization to host porphyry emplacement: Re–Os ages of molybdenites versus U–Pb ages of zircons and sulfur isotope compositions of pyrite and chalcopyrite from the Iju and Sarkuh porphyry deposits in southeast Iran. Economic Geology 108, 861–870.

Mohajjel, M., Fergusson, C.L., Sahandi, M.R., 2003. Cretaceous-Tertiary convergence and continental collision, Sanandaj-Sirjan zone, western Iran. Asian Earth Science 21, 397–412.

Nabatian, G., Ghaderi, M., Neubauer, F., Honarmand, M., Liu, X., Dong, Y., Jiang, S., Quadt, A., Bernroide, M., 2014. Petrogenesis of Tarom high-potassic granitoids in the Alborz-Azarbaijan belt, Iran: geochemical, U–Pb zircon and Sr–Nd–Pb isotopic constraints. Lithos 184–187, 324–345.

Pang, K.-N., Chung, S.-L., Zarrinkoub, M.H., Khatib, M.M., Mohammadi, S.S., Chiu, H.-Y., Chu, C.-H., Lee, H.-Y., Lo, C.-H., 2013. Eocene-Oligocene post-collisional magmatism in the Lut-Sistan region, eastern Iran: Magma genesis and tectonic implications. Lithos 180–181, 234–251.

Pang, K.-N., Chung, S.-L., Zarrinkoub, M.H., Mohammadi, S.S., Yang, H.-M., Chu, C.-H., Lee, H.-Y., Lo, C.-H., 2012. Age, geochemical characteristics and petrogenesis of Late Cenozoic intraplate alkali basalts in the Lut–Sistan region, eastern Iran. Chemical Geology 306–307, 40–53.

Pearce, J.A., Harris, N.B.W., Tindle, A.G., 1984. Trace element discrimination diagrams for the tectonic interpretation of granitic rocks. Petrology 25, 956–983.

Pearce, J.A., Peate, D.W., 1995. Tectonic implications of the composition of volcanic arc magmas. Annual Review of Earth and Plaentary Sciences 23, 251–285.

Peccerillo, A., Taylor, S.R., 1976. Geochemistry of Eocene calc-alkaline volcanic rocks from the Kastamonu area (Northern Turkey). Contributions to Mineralogy and Petrology 58 (1), 63–81.

Petford, N., Atherton, A., 1996. Na-rich partial melts from newly underplated basaltic crust: the Cordillera Blanca batholith, Peru. Petrology 37, 1491–1521.

Rapp, R.P., Watson, E.B., 1995. Dehydration melting of metabasalt at 8–32 kbar: implications for continental growth and crust–mantle recycling. Petrology 36, 891–931.

Richards, J.P., Spell, T., Rameh, E., Razique, A., Fletcher, T., 2012. High Sr/Y reflect arc maturity, high magmatic water content, and porphyry Cu ± Mo ± Au potential: examples from the Tethyan arcs of central and eastern Iran western Pakistan. Economic Geology 107, 295–332.

Rollinson, H.R., 1993. Using Geochemical Data: Evaluation, Presentation, Interpretation, Longman Science and Technical, 352 p.

Rowshanravan, J., 2006. Geochemical map of Mousaviyeh Sheet (1:100,000), Geological Survey of Iran, Tehran.

Rudnick, R.L., 1995. Making continental crust. Nature 378, 571–578.

Salim, L., 2012. Geology, petrology and geochemistry of volcanic and sub volcanic rocks in Cheshme Khuri area (North West of Birjand). MSc thesis. Birjand University, Iran.

Schandl, E.S., Gorton, M.P., 2002. Application of high field strength elements to discriminate tectonic settings in VMS environments. Economic Geology 97, 629–642.

Shafiei, B., Shahabpour, J., Haschke, M., 2008. Transition from Paleogene normal calcalkaline to neogene adakitic-like plutonism and Cu-metallogeny in the Kerman porphyry copper belt: response to neogene crustal thickening. Iranian Journal of Science 19, 67–84.

Shah. A., Bedrosian. P., Anderson. E., Kelley. K., Lang. J., 2013. Integrated geophysical imaging of a concealed mineral deposit: A case study of the world-class Pebble porphyry deposit in southwestern Alaska. Geophysics 78 (5), 317-328.

Shahabpour, J., 2007. Island-arc affinity of the Central Iranian Volcanic Belt. Asian Earth Science 30, 652–665.

Simmons, S.F., Christenson, B.W., 1994. Origins of calcite in a boiling geothermal system. American Journal of Science 294 (3), 361–400.

Stern, C.R., Kilian, R., 1996. Role of the subducted slab, mantle wedge and continental crust in the generation of adakites from the Andean Austral Volcanic Zone. Contributions to Mineralogy and Petrology 123, 263–281.

Stolz, A.J., Jochum, K.P., Spettel, B., Hofman, A.W., 1996. Fluid and meltrelated enrichment in the subarc mantle: evidence from Nb/Ta variations in island-arc basalts. Geology 24, 587–590.

Sun, S.S., McDonough, W.F., 1989. Chemical and isotopic systematics of oceanic basalts: implications for mantle composition and processes. Geological Society of London Special Publication. 42, 313–345.

Tarkian, M., Lotfi, M., Baumann, A., 1983. Tectonic, magmatism and the formation of mineral deposits in the central Lut, east Iran, Ministry of mines and metals, Geological Survey of Iran, Geodynamic Project (Geotraverse) in Iran. 51, 357–383.

Taylor, S.R., McLennan, S.M., 1985. The Continental Crust: Its Composition and Evolution. Blackwell, Oxford.

Tirrul, R., Bell, I.R., Griffis, R.J., Camp, V.E., 1983. The Sistan suture zone of eastern Iran. Geological Society of America Bulletin 94, 134–150.

Vervoort, J.D., Patchett, P.J., Blichert- Toft, J., Albarede, F., 1999. Relationship between Lu-Hf and Sm-Nd isotopic systems in the global sedimentary system. Earth and Planetary Science Letters 168, 79–99.

Villa, I.M., De Bièvre, P., Holden, N.E., Renne, P.R., 2015. IUPAC-IUGS recommendation on the half-life of ^{87}Rb. Geochimica and Cosmochimica Acta 164, 382–385.

Whalen, J.B., Currie, K.L., Chappell, B.W., 1987. A-type granites: geochemical characteristics, discrimination and petrogenesis. Contributions to Mineralogy and Petrology 95, 407–419.

Whitney, D.L., Evans, B.W., 2010. Abbreviations for names of rock-forming minerals. American Mineralogist 95: 185–187.

Wilson, M., 1989. Igneous Petrogenesis: A Global Tectonic Approach. Harper Collins Academic, New York.

Xu, Y.M., Jiang, S.Y., Zhu, Z.Y., Yang, S.Y., Zhou, W., 2014. Petrogenesis of Late Mesozoic granitoids and coeval mafic rocks from the Jiurui district in the Middle-Lower Yangtze metallogenic belt of Eastern China: geochemical and Sr– Nd–Pb–Hf isotopic evidence. Lithos 467–484.

Yang, J.H., Wu, F.Y., Wilde, S.A., Xie, L.W., Yang, Y.H., Liu, X.M., 2007. Tracing magma mixing in granite genesis, in situ U–Pb dating and Hf-isotope analysis of zircons. Contributions to Mineralogy and Petrology 153 (2), 177–190.

Zarrinkoub, M.H., Chung, S.-L., Chiu, H.-Y., Mohammadi, S., Khatib, M., Lin, I.-J., 2010. Zircon U\Pb age and geochemical constraints from the northern Sistan suture zone on the Neotethyan magmatic and tectonic evolution in eastern Iran. Abstract to GSA Conference on “Tectonic Crossroads: Evolving Orogens in Eurasia–Africa–Arabia”, Oct. 4–8, 2010, 520 Ankara, Turkey.

Zarrinkoub, M.H., Pang, K.-N., Chung, S.-L., Khatib, M.M., Mohammadi, S.S., Chiu, H.-Y., Lee, H.-Y., 2012. Zircon U\Pb age and geochemical constraints on the origin of the Birjand ophiolite, Sistan suture zone, eastern Iran. Lithos 154, 392–405.

Zhang, H., Zhang, L., Harris, N., Jin, L., Honglin, Y., 2006. U–Pb zircon ages, geochemical and isotopic compositions of granitoids in Songpan-Garze fold belt, eastern Tibetan Plateau: constraints on petrogenesis and tectonic evolution of the basement. Contributions to Mineralogy and Petrology 152 (1), 75–88.

Highlights

- Cheshmeh Khuri prospect area is a porphyry copper mineralization in the Lut Block, Eastern Iran.
- We studied the age, genesis and geodynamic control of the magmatism in Cheshmeh Khuri prospecting area.
- The subvolcanic rocks related to mineralization have features typical of high-K calk-alkaline and belong to magnetite granitoid series (I-type).
- Magmas of Cheshmeh Khuri area formed in a subduction-modified upper mantle in post-collisional extension-related zone.